NASA Technical Paper 3324

July 1993

Geometric Model From Microscopic Theory for Nuclear Absorption

Sarah John,
Lawrence W. Townsend,
John W. Wilson,
and Ram K. Tripathi

NASA

NASA Technical Paper 3324

1993

Geometric Model From Microscopic Theory for Nuclear Absorption

Sarah John
ViGYAN, Inc.
Hampton, Virginia

Lawrence W. Townsend
and John W. Wilson
Langley Research Center
Hampton, Virginia

Ram K. Tripathi
ViGYAN, Inc.
Hampton, Virginia

National Aeronautics and Space Administration
Office of Management
Scientific and Technical Information Program

Abstract

A parameter-free geometric model for nuclear absorption is derived herein from microscopic theory. The expression for the absorption cross section in the eikonal approximation, taken in integral form, is separated into a geometric contribution that is described by an energy-dependent effective radius and two surface terms that cancel in an asymptotic series expansion. For collisions of light nuclei, an expression for the effective radius is derived from harmonic oscillator nuclear density functions. A direct extension to heavy nuclei with Woods-Saxon densities is made by identifying the equivalent half-density radius for the harmonic oscillator functions. Coulomb corrections are incorporated, and a simplified geometric form of the Bradt-Peters type is obtained. Results spanning the energy range from 1 MeV/nucleon to 1 GeV/nucleon are presented. Good agreement with experimental results is obtained.

Introduction

The nuclear absorption cross section is a measure of the sum of all the reaction processes induced during nuclear collisions. This metric is applied widely in such diverse fields as fundamental nuclear physics, the study of radiation effects on living cells, and radiation-shielding design for future space-exploration vehicles (ref. 1).

In recent years, considerable advancements in both the theory (refs. 2–19) and experimental methods (refs. 20–26) of this fundamental observable have been made. Most significantly, the energy variations of the absorption cross sections for all nuclei in the intermediate-energy range from 10 MeV/nucleon to 1 GeV/nucleon are qualitatively similar and can be related to the underlying two-nucleon interactions. At energies above 1 GeV/nucleon, the absorption cross section is essentially constant and approximately equals the total geometric cross-sectional area of the projectile-target system; this consistency allows an extension of the geometric model and its parameterized forms (refs. 13–17, 25, and 26) to the entire intermediate- and low-energy range. The geometric formula provides a quick method for the calculation of the absorption cross section and is highly desirable for inclusion in radiation-shielding transport codes.

Microscopic formulations are based on the quantum collision theory of many-body composite systems. The solution of this complex problem can be approached with the methods of Glauber (ref. 2), Watson (ref. 3), Feshbach (ref. 3), and the KMT approach (ref. 4). Wilson (ref. 5) extended the Watson formalism of nucleon-nucleus collisions to nucleus-nucleus collisions, from which the cross sections in the eikonal approximation can be obtained. These solutions, which are generally solved by numerical methods (refs. 5 and 6), are given in integral form.

Closed-form solutions for the microscopic theory have been obtained for the simplest case of Gaussian nuclear density distribution (refs. 7 and 8). The solution applicability to the more realistic density distribution of the Woods-Saxon form is based on matching equivalent Gaussian forms to the surface densities of heavier nuclei. This approach is successful because the energy dependence for the transparency is largely a function of the low-density surface region with a saturated, absorptive inner core that remains essentially energy independent.

The purpose of this paper is to derive a geometric formula, valid for both light and heavy nuclei, for the nuclear absorption cross section from the microscopic formulation. This effort will be accomplished by separating the integral expression for the absorption cross section in the eikonal approximation into an effective geometric radius and two surface components that approximately cancel in the asymptotic expansion.

The concept of the effective radius in microscopic formulations is not new (refs. 8 and 9). However, in all previous works the contributions beyond a cutoff radius are negligible, whether the effective radius is defined at half-absorption density (ref. 8) or at a distance of one mean free path from the surface (ref. 9). In this work, however, the effective radius at half-absorption density has a precise definition such that the transparency within this radius cancels the absorptive contribution from the outer region.

A summary of the format for this paper is presented. In "Theory," the results from the microscopic theory are reviewed and developed into a geometric formalism. In "Application to Light Nuclei," a method is illustrated for harmonic oscillator matter densities that are applicable to light nuclei. Expressions for the eikonal phase shift and the total absorption cross section are derived for the nucleon-nucleus as well as for the nucleus-nucleus interactions. An exact formula for the effective radius at half absorption is derived, and its first approximation is used to evaluate explicitly the geometric term and the surface contributions. Results comparing experiments for energy values from 50 MeV/nucleon to 1 GeV/nucleon are presented. Also, a simplified version of the expression for the effective radius, which is used in the rest of the sections, is given. In "Extension to Woods-Saxon Densities," a direct

extension of the expression mentioned above is made for the heavier nuclei described by Woods-Saxon density distributions. In "Coulomb Interactions," the effects of Coulomb deflections are incorporated, and results for light- and heavy-ion projectile-target systems spanning the energy range from 1 MeV/nucleon to 1 GeV/nucleon are presented. In "Bradt-Peters Form," the expressions are further simplified and the results compared with those of the previous section. In "Nuclear-Medium Effects," comments are made on nuclear-medium effects. "Concluding Remarks" summarizes the suggestions for improvement submitted herein.

Theory

Microscopic Theory

The nuclear absorption cross section in the eikonal approximation is given by

$$\sigma_{\text{abs}} = 2\pi \int_0^\infty \{1 - \exp[-2\text{Im } \chi(b,e)]\} b \, db \qquad (1)$$

where Im denotes the imaginary part of the complex phase shift $\chi(b,e)$, which is a function of the impact parameter b and energy e, and can be derived from a multiple-scattering series expansion for the optical potential (refs. 5 and 6). Within the Watson form of impulse approximation, when the propagator G is replaced by the free propagator G_o (ref. 5), the phase shift is given by

$$\chi(b,e) = \frac{A_P^2 A_T^2}{k(A_P + A_T)} \int dz \int d^3\xi \rho_T(\boldsymbol{\xi}) \times \int d^3y \rho_P(\mathbf{b} + z + \mathbf{y} + \boldsymbol{\xi}) t(e,\mathbf{y}) \qquad (2)$$

where k is the wave number of the projectile, A_P and A_T are the mass numbers, and ρ_P and ρ_T are the projectile and matter densities; $t(e,\mathbf{y})$ signifies the two-body transition amplitude for free nucleons as follows:

$$t(e,\mathbf{y}) = -\left(\frac{e}{m}\right)^{1/2} \bar{\sigma}(e)\,[\alpha(e) + i]\,[2\pi\ B(e)]^{-3/2} \times \exp\left[-\frac{\mathbf{y}^2}{2B(e)}\right] \qquad (3)$$

Here, e is the two-nucleon kinetic energy in the center-of-mass (cm) frame of reference, m is the nucleon rest mass, $\bar{\sigma}(e)$ is the isospin-averaged total nucleon-nucleon cross section, $B(e)$ is the averaged slope parameter, and $\alpha(e)$ is the averaged ratio of the real to imaginary components of the forward-scattering amplitudes.

Geometric Model

A geometric formula for the absorption cross section of high-energy nuclear collisions is given by the Bradt-Peters form (ref. 2),

$$\sigma_{\text{abs}} = \pi\,(R_P + R_T - \delta_o)^2 \qquad (4)$$

where R_P and R_T are the radii of the projectile and target nuclei and δ_o is a constant. If δ_o is small compared with the radii, the formula shown above implies an annular region of transparency for peripheral collisions. To show that this form may indeed be derived from microscopic theory, the integral given in equation (1) is separated at an impact parameter R_e as follows:

$$\begin{aligned}\sigma_{\text{abs}} &= 2\pi \int_0^{R_e} \{1 - \exp[-2\text{Im}\chi(b,e)]\}\, b\, db \\ &\quad + 2\pi \int_{R_e}^\infty \{1 - \exp[-2\text{Im}\chi(b,e)]\}\, b\, db \\ &= \pi R_e^2 - \delta_1 + \delta_2 \end{aligned} \qquad (5)$$

such that δ_1 and δ_2 are the small surface contributions given by

$$\delta_1 = 2\pi \int_o^{R_e} \exp[-2\text{Im}\chi(b,e)]\, b\, db \qquad (6)$$

and

$$\delta_2 = 2\pi \int_{R_e}^\infty \{1 - \exp[-2\text{Im}\chi(b,e)]\}\, b\, db \qquad (7)$$

Appendix A includes the asymptotic series expansions,

$$\delta_1 \approx 2\pi R_e \frac{\exp[-\chi_1(R_e,e)]}{\partial\chi_1(b,e)/\partial b|_{R_e}} \qquad (8)$$

and

$$\delta_2 \approx 2\pi R_e \frac{\{1 - \exp[-\chi_1(R_e,e)]\}^2}{\partial\chi_1(b,e)/\partial b|_{R_e}} \exp[\chi_1(R_e,e)] \qquad (9)$$

where

$$\chi_1(b,e) = 2\text{Im}\chi(b,e) \qquad (10)$$

Note that δ_2 can also be expanded into a convergent Taylor series, provided that $\chi_1(b,e) < 1$ beyond

R_e and that, in the first approximation, δ_2 is given by

$$\delta_2 \approx \int_{R_e}^{\infty} \chi_1(b,e) b \, db \tag{11}$$

From equations (8) and (9),

$$\delta_2 - \delta_1 = 2\pi R_e \delta(R_e, e) \tag{12}$$

where

$$\delta(R_e,e) = \frac{\exp[\chi_1(R_e,e)]}{\partial\chi_1(b,e)/\partial b|_{R_e}} \{1 - 2\exp[-\chi_1(R_e,e)]\} \tag{13}$$

Hence,

$$\begin{aligned} \sigma_{\text{abs}} &= \pi R_e^2 - 2\pi R_e \delta(R_e,e) \\ &\approx \pi[R_e - \delta(R_e,e)]^2 \end{aligned} \tag{14}$$

If the integration limit R_e is the sum of the projectile and target radii, the required geometric formula shown in equation (4) is obtained. However, for convenience, R_e can be chosen such that δ is identically zero. When this condition is valid, equation (13) shows

$$\exp[-\chi_1(R_e,e)] = 0.5$$

or

$$\chi_1(R_e,e) = \ln 2 \tag{15}$$

That is, R_e is chosen at half transparency or, equivalently, at half absorption. (See fig. 1.) The transparency function T is

$$T = \exp[-\chi_1(b,e)] \tag{16}$$

and the absorption function $A = 1 - T$. With $\delta \equiv 0$,

$$\sigma_{\text{abs}} = \pi R_e^2 \tag{17}$$

where the effective radius R_e is now a function of energy. This equation gives the desired geometric formula for the nuclear absorption; R_e is derived from equation (15). However, a more appropriate formula for R_e can be derived in terms of the classical geometric radius R_g, which is defined as $R_{e\to\infty}$. Note that at the high-energy limit, as $e \to \infty$, the wavelength of the projectile nucleons is sufficiently small compared with the nuclear dimensions, and the effective radius assumes the classical geometric radius R_g, given by

$$R_g = r_o\left(A_P^{1/3} + A_T^{1/3}\right) \tag{18}$$

where r_o is a variable determined by the condition

$$\chi_1(R_g,\infty) = \ln 2 \tag{19}$$

such that $\delta = 0$ is satisfied. The effective radius R_e at an arbitrary energy e can then be related to the geometric radius R_g by equating

$$\chi_1(R_e,e) = \chi_1(R_g,\infty) = \ln 2 \tag{20}$$

This relation is useful only if an algebraic expression for $\chi(b,e)$ is known. For Gaussian and harmonic oscillator density functions, $\chi(b,e)$ is readily obtained by the methods in "Application to Light Nuclei."

Application to Light Nuclei

In this section, the phase-shift function $\chi(b,e)$ is derived from the harmonic oscillator density function, which is applicable to light nuclei for $A \le 16$. Also, an exact expression for the effective radius is obtained. The nucleon-nucleus and nucleus-nucleus collisions are treated separately.

For the nucleon-nucleus collision, the nucleon density is simply

$$\rho(x - x') = \delta(x - x') \tag{21}$$

because the nucleon wave function has been effectively incorporated into the two-body transition amplitude $t(e,\mathbf{y})$, and the nucleus charge density is given by

$$\rho_c(x) = \rho_o\left(1 + \gamma\frac{x^2}{a^2}\right)\exp\left(-\frac{x^2}{a^2}\right) \tag{22}$$

where γ and a fm (1 fermi $= 1 \times 10^{-15}$ m) are constants taken from reference 27. The expression for $\chi(b,e)$ is derived in appendix B and has the following form for the nucleon-nucleus system:

$$\chi_1(b,e) = f_1(e)\left(a_1 + a_2 b^2\right)\exp[-P(e)b^2] \tag{23a}$$

and for the nucleus-nucleus system:

$$\chi_1(b,e) = f_1(e)\left(a_1 + a_2 b^2 + a_3 b^4\right)\exp[-P(e)b^2] \tag{23b}$$

where explicit expressions for the functions $f_1(e)$ and $P(e)$ and for the constants a_1, a_2, and a_3 in each case are given in appendix B.

Figure 2 displays the absorption function

$$A = 1 - \exp[-\chi_1(b,e)] \tag{24}$$

as a function of the impact parameter b, for ^{4}He–^{4}He and ^{16}O–^{16}O systems, at an energy of 2 GeV/nucleon, which is taken as the geometric limit. The position of the effective radius R_e that is defined at $T = A = 0.5$

is also indicated. Note that even within the geometric limit, considerable transparency for peripheral collisions occurs.

The effective radius R_e for three different energy values is shown in figure 3, where the absorption is plotted at 50 MeV/nucleon, 250 MeV/nucleon, and 1 GeV/nucleon for the ^{16}O–^{16}O system. As shown in the figure, R_e passes through a minimum and then increases as the energy decreases. The strong absorption radius R_s is reached in the low-energy limit. The underlying basis for this energy dependence can be traced to the nucleon-nucleon total cross section, which exhibits a similar trend. An expression for the effective radius R_e in terms of its geometric value R_g is obtained from equations (23) and the condition

$$\chi_1(R_e, e) = \chi_1(R_g, \infty)$$

For nucleus-nucleus collisions,

$$R_e^2 = \frac{P(\infty)}{P(e)} R_g^2 + \frac{1}{P(e)} \left\{ \ln\left[\frac{f_1(e)}{f_1(\infty)}\right] + \ln\left(\frac{a_1 + a_2 R_e^2 + a_3 R_e^4}{a_1 + a_2 R_g^2 + a_3 R_g^4}\right) \right\} \tag{25}$$

with a similar expression for the nucleon-nucleus case for $a_3 = 0$. In the equation above, the geometric value R_g is given by

$$R_g = r_T A_T^{1/3} \tag{26a}$$

for the nucleon-nucleus system and

$$R_g = r_T A_T^{1/3} + r_P A_P^{1/3} \tag{26b}$$

for the nucleus-nucleus system. The value r is determined from the condition

$$\chi(R_g, 2A \text{ GeV}) = \ln 2$$

which, for the nucleus-nucleus system, is given by

$$\ln f_1(2A \text{ GeV}) + \ln\left(a_1 + a_2 R_g^2 + a_3 R_g^4\right) - P(2A \text{ GeV}) R_g^2 = \ln(\ln 2) \tag{27}$$

Substituting for R_g from equation (26), equation (27) is solved iteratively with an initial value of $r_o = 1.0$ fm. For the nucleus-nucleus system, identical target-projectile systems are considered with $r_T = r_P = r_o$. The resulting values for r_o are plotted in figure 4 and listed in table I. From equation (20), this determination is clearly sufficient to ensure that the condition $\delta = 0$ is also satisfied by the value of the effective radius given by equation (25).

Table I. Collision Values for r_o

Atomic mass number	r_o, fm	
	Nucleon-nucleus	Nucleus-nucleus
2	0.50	0.47
4	1.02	0.85
7	1.14	1.13
9	1.19	1.17
10	1.19	1.16
11	1.18	1.14
12	1.19	1.13
14	1.20	1.16
16	1.23	1.21
>16	1.25	1.25

For the heavier nuclei within the harmonic oscillator category, $r_o \approx 1.2$ fm; this length approximates the generally accepted value that determines the nuclear radius. Clearly, the values of r_o for the lightest nuclei such as deuterium and helium are considerably smaller than those for the heavier nuclei; this difference can be explained by examining the convolution integral for the phase shift. In the case of Gaussian density distributions, the resultant width increases by the factor $\left(a_P^2 + a_T^2\right)^{1/2}$, whereas the total geometric width is given by the sum $a_P + a_T$, as shown in equation (26), where a_P and a_T are the widths of the target and projectile, respectively. Hence, for the lightest nuclei, which have near-Gaussian distributions, r_o must be lowered to account for this discrepancy. The convolution widths for the Woods-Saxon forms, however, are expected to be close to the geometric value.

The advantage of writing R_e in terms of R_g, as given in equation (25), is that in the first approximation the second logarithmic term may be neglected when $R_e \approx R_g$, with the result

$$R_e^2 \approx \frac{P(2A \text{ GeV})}{P(e)} R_g^2 + \frac{1}{P(e)} \ln\left[\frac{f_1(e)}{f_1(2A \text{ GeV})}\right] \tag{28}$$

Although this approximation offsets the condition $\delta = 0$, the integration limit in equation (5) is sufficiently defined to evaluate δ_1 and δ_2 explicitly; the absorption cross section is given accurately by

$$\sigma_{\text{abs}} = \pi R_e^2 - \delta_1(R_e, e) + \delta_2(R_e, e) \tag{29}$$

Figures 5–9 display the absorption cross section using equation (29) for light-ion projectile-target systems that agree well with experimental data. These results are also in close agreement with the numerical evaluation of the integral given by equation (1). (See refs. 5 and 6.)

Hereafter, the expression for R_e from equation (28) will be used with the assumption that $(\delta_2 - \delta_1)$ is negligible. In equation (28), the expression $P(e)$ for the nucleon-nucleus collision is equivalent to equation (B10),

$$P(e) = \left[a_T^2 - \frac{2}{3}r_p^2 + 2B(e)\right]^{-1} \tag{30a}$$

and $P(e)$ for nucleus-nucleus collision is equivalent to equation (B17),

$$P(e) = \left[a_T^2 + a_P^2 - \frac{4}{3}r_p^2 + 2B(e)\right]^{-1} \tag{30b}$$

where $r_p = 0.86$ fm is the radius of the proton. Because the slope parameter $B(e)$ is approximately a constant equal to 0.4 fm^2 within the energy range considered, $P(2A \text{ GeV}) \approx P(e)$; equation (28), with R_g given by equation (26), then simplifies to

$$R_e^2 = \left(r_T A_T^{1/3}\right)^2 + \left(a_T^2 + 0.35\right) g(e) \tag{31a}$$

for the nucleon-nucleus collision, and

$$R_e^2 = \left(r_P A_P^{1/3} + r_T A_T^{1/3}\right)^2 + \left(a_T^2 + a_P^2\right) g(e) \tag{31b}$$

for the nucleus-nucleus collision, where

$$g(e) = \ln\left[\frac{f_1(e)}{f_1\ (2A \text{ GeV})}\right]$$

$$\approx \ln\left[\frac{\bar{\sigma}(e)}{\bar{\sigma}(2A \text{ GeV})}\right] \tag{32}$$

The terms A_P and A_T are the charge density width parameters for the harmonic oscillator function given in reference 27, r_P and r_T are the respective values for r_o given in table I, and the parameterized form for $\bar{\sigma}(e)$ is given in appendix C.

Extension to Woods-Saxon Densities

The Woods-Saxon density does not yield a simple expression for the phase shift $\chi(b, e)$. Therefore, a simple modification of equations (31) is given. The two-parameter Woods-Saxon charge density is given by

$$\rho_c(r) = \frac{\rho_o}{1 + \exp\left(\frac{r - R}{c}\right)}$$

where R is the radius at half density, c is related to the nuclear skin thickness t by the expression $c = t/4.4$, and ρ_o is a normalization constant. From reference 27, the parameter c is a constant approximately equal to 0.55 fm for all nuclei. Hence, we assume that only one parameter R describes the Woods-Saxon form.

The equivalent half-density distance R for the harmonic oscillator function satisfies

$$\frac{1}{2} = \left(1 + \gamma\frac{R^2}{a^2}\right)\exp\left(-\frac{R^2}{a^2}\right) \tag{33}$$

which can be rewritten as

$$k = \ln 2 + \ln(1 + \gamma k) \tag{34}$$

where

$$k = \frac{R^2}{a^2} \tag{35}$$

Equation (34) is solved iteratively for k with an initial value of $k = \ln 2$. The parameter k is plotted in figure 10 as a function of atomic mass number. For the heavier nuclei with the harmonic oscillator density form, $k \approx 2$ or $R \approx \sqrt{2}a$. Also, for these nuclei an equally valid description would be the Woods-Saxon form with the half-density radius given by $R = \sqrt{2}a$. This equivalence suggests that the substitution of

$$a = \frac{R}{\sqrt{2}}$$

into equations (31) can extend its range of applicability to the Woods-Saxon densities of heavy ions with $A > 16$. This substitution yields for the nucleon-nucleus system,

$$R_e^2 = \left(r_T A_T^{1/3}\right)^2 + \left(\frac{R_T^2}{2} + 0.35\right) g(e) \tag{36a}$$

and for the nucleus-nucleus system,

$$R_e^2 = \left(r_P\ A_P^{1/3} + r_T A_T^{1/3}\right)^2 + \frac{1}{2}\left(R_T^2 + R_P^2\right) g(e) \tag{36b}$$

where R_P and R_T are the half-density values for the Woods-Saxon forms given in reference 27.

Coulomb Interactions

The derivation of the eikonal approximation assumes straight-line trajectories for the projectile and an impact parameter at the collision site that is equal to its asymptotic value. For heavy ions at low energy, the Coulomb force deflects the straight-line trajectories significantly, thereby decreasing the cross-sectional area of incident particles that actually undergo nuclear forces. The eikonal approximation may still be used (refs. 8, 10, and 18) if the effective impact parameter at the collision site is the distance of closest approach d (refs. 8 and 18), where b and d are related by

$$b^2 = d^2\left(1 - \frac{2a}{d}\right) \tag{37}$$

with

$$a = \frac{Z_T Z_P e_o^2}{E_{\text{cm}}}$$

where Z_T and Z_P are the charges of the target and projectile, respectively, e_o is the electron charge, and E_{cm} is the total center-of-mass energy.

Hence, the asymptotic impact parameter b_e, corresponding to the radial distance R_e, is given by

$$b_e^2 = R_e^2\left(1 - \frac{2a}{R_e}\right) \tag{38}$$

where b_e now defines the integration limit for equation (5). Therefore, the Coulomb-modified geometric formula is readily obtained as

$$\sigma_{\text{abs}} = \pi R_e^2\left(1 - \frac{2a}{R_e}\right) \tag{39}$$

In figures 11–21, the absorption cross section for several light- and heavy-ion projectile-target nuclei is plotted with and without the Coulomb corrections for energy values from 1 MeV/nucleon to 2 GeV/nucleon. The results with Coulomb corrections agree well with experiment. The following values for r_o (see table I) were used for nucleus-nucleus collisions:

$$\begin{aligned} A = 4; &\quad r_o = 0.56 \text{ fm} \\ 7 < A < 16; &\quad r_o = 1.20 \text{ fm} \\ A > 16; &\quad r_o = 1.25 \text{ fm} \end{aligned}$$

Figures 22–26 show the cross sections for specific projectiles on various targets with and without Coulomb interaction. The linear relationship with atomic number is clearly evident. As expected, the Coulomb corrections are more significant for heavy ions.

Bradt-Peters Form

In the present formalism, the geometric limit for the nuclear absorption cross section is given by

$$\sigma_{\text{abs}} = \pi r_o^2\left(A_P^{1/3} + A_T^{1/3}\right)^2$$

compared with the Bradt-Peters form at high energy,

$$\sigma_{\text{abs}} = \pi r_o^2\left(A_P^{1/3} + A_T^{1/3} - \delta_o\right)^2$$

The difference comes from the choice of r_o. Here, r_o satisfies the geometric criteria that are valid at high energies and small wavelengths such that

$$R_g = r_o\left(A_P^{1/3} + A_T^{1/3}\right) \quad (T = 0.5; e \to \infty)$$

An equally valid description is to define the strong absorption radius R_s at low energy as the reference value such that

$$R_s = r_s\left(A_P^{1/3} + A_T^{1/3}\right) \quad (T = 0.5; e \to 0)$$

The strong absorption parameter r_s is greater than r_o because the absorptive content of the surface region increases at lower energies due to s-wave scattering. This low-energy description results in $\delta_o \neq 0$ at high energy, a state that conforms to the Bradt-Peters formula.

However, since the eikonal approximation is valid only at high energies, the low-energy description cannot be implemented. Also, the corrections that show the Coulomb and Pauli correlation, significant contributors at low energies, were not incorporated into the phase-shift function. Hence, the choice of the geometric limit as the reference point is justified.

The more general equations (36) for the effective radius R_e at intermediate energy will now be cast in the Bradt-Peters form. The simplest form is obtained for heavy ions when $r_T = r_P = r_o$. Using the parameterized form for half-density charge radius R, given by

$$R = c_1 A^{1/3} - c_2$$

with

$$\left.\begin{aligned} c_1 &= 1.18 \\ c_2 &= 0.48 \end{aligned}\right\} \tag{40}$$

in equations (36) and simplifying, the Bradt-Peters form is obtained for the nucleon-nucleus system

$$R_e^2 = r^2(e)\left[A_T^{1/3} - \delta_o(e)\right]^2 \qquad (41a)$$

where

$$r^2(e) = r_o^2 + \frac{c_1^2\, g(e)}{2}$$

$$\delta_o(e) \approx \frac{g(e)}{2r^2(e)}\, c_1 c_2$$

and for the nucleus-nucleus system as

$$R_e^2 = r^2(e)\left[A_P^{1/3} + A_T^{1/3} - \delta_o(A_P, A_T, e)\right]^2 \qquad (41b)$$

with r as shown before and

$$\delta_o(A_P, A_T, e) \approx \frac{g(e)}{2r^2(e)}\left(c_1 c_2 + c_1^2 \frac{A_T^{1/3} A_P^{1/3}}{A_T^{1/3} + A_P^{1/3}}\right)$$

where $r_o = 1.25$ fm.

In deriving the formula above, δ_o is assumed to be much smaller than $A_P^{1/3}$ and $A_T^{1/3}$. Note that r is now energy dependent, which supports the observation made by Kox et al. (ref. 25).

After the above equation is substituted into equation (39) to account for Coulomb correction, the results are compared with those of the previous section in figures 27–30. The agreement is good for the heavier as well as for the proton projectiles. The discrepancy for the alpha projectiles in the nucleus-nucleus case results from the assumption $r_P = r_T = 1.25$ fm for all nuclei in the Bradt-Peters form.

Nuclear-Medium Effects

In the microscopic formulation, the two-nucleon interaction is defined between free nucleons. This definition excludes nuclear-medium effects from Fermi motion and Pauli blocking. The exclusion of these effects can be justified in both the high- and low-energy (below $20A$ MeV) regimes but not in the intermediate-energy region. At high energy, many scattering states are available; hence, the effects of the occupied states are comparatively negligible. At low energy, peripheral collisions dominate when the nuclear overlap densities are low and when the number of occupied states is small. Peripheral collisions dominate at low energies for the following reasons: the nuclear absorptive power increases due to s-wave scattering between nucleons, and Coulomb forces deflect the trajectories into the peripheral regions. Thus, reasonably good results are obtained with the Coulomb corrections alone. The nuclear-medium effects should actually increase the mean free paths (ref. 19); hence, more nuclear transparency results. For uncharged projectiles such as the neutron, these effects can be considerable, as shown in figure 14(b).

Concluding Remarks

A parameter-free geometric model for nuclear absorption was derived herein from microscopic theory. The expression for the absorption cross section in the eikonal approximation, taken in integral form, was separated into a geometric contribution that was described by an energy-dependent effective radius and two surface terms that cancelled in an asymptotic series expansion.

For collisions of light nuclei, an expression for the effective radius was derived from harmonic oscillator nuclear density functions. A direct extension to heavy nuclei with Woods-Saxon densities was made by identifying the equivalent half-density radius for the harmonic oscillator functions. Coulomb corrections were incorporated, and a simplified geometric form of the Bradt-Peters type was obtained. Results spanning the energy range from 1 MeV/nucleon to 1 GeV/nucleon were presented. Good agreement with experimental results was obtained.

NASA Langley Research Center
Hampton, VA 23681-0001
April 23, 1993

Appendix A

Surface Contributions to Total Absorption Cross Section

The surface contributions to the total absorption cross section, given by δ_1 and δ_2, are evaluated using the Laplace method for asymptotic series (ref. 27)

$$\begin{aligned}\delta_1 &= 2\pi \int_o^{R_e} \exp[-\chi_1(b,e)] b \, db \\ &= 2\pi \int_o^{R_e} \exp\left\{ - \left[\chi_1(R_e,e) + \frac{\partial \chi_1(b,e)}{\partial b}(b - R_e) + \ldots \right] \right\} b \, db \\ &\approx 2\pi R_e \frac{\exp[-\chi_1(R_e,e)]}{\partial \chi_1(b,e)/\partial b|_{R_e}}\end{aligned} \tag{A1}$$

Similarly,

$$\begin{aligned}\delta_2 &= 2\pi \int_{R_e}^{\infty} \{1 - \exp[-\chi_1(b,e)]\} b \, db \\ &= 2\pi \int_{R_e}^{\infty} \exp\big(\ln \{1 - \exp[-\chi_1(b,e)]\} \big) b \, db \\ &= 2\pi \int_{R_e}^{\infty} \exp\left[\ln\{1 - \exp[-\chi_1(R_e,e)]\} + \frac{\partial}{\partial b} \left(\ln\{1 - \exp[-\chi_1(b,e)]\} \right) (b - R_e) + \ldots \right] b \, db \\ &\approx 2\pi R_e \frac{\{1 - \exp[-\chi_1(R_e,e)]\}^2}{\exp[\chi_1(R_e,e)][\partial \chi_1(b,e)/\partial b]|_{R_e}}\end{aligned} \tag{A2}$$

Appendix B

Derivation for Phase Shift $\chi(b,e)$

Expressions for the phase shift $\chi(b,e)$ are derived from the harmonic oscillator density functions. The charge density is

$$\rho_c(x) = \rho_o\left(1+\gamma\frac{x^2}{a^2}\right)\exp\left(-\frac{x^2}{a^2}\right) \tag{B1}$$

where γ and a fm are taken from reference 27 and ρ_o is a normalization factor.

The matter density is derived from the charge density (ref. 29) as

$$\rho_m(x) = \rho_o(a' + b'x^2)\exp(-px^2) \tag{B2}$$

where

$$a' = \frac{a^3}{8s^3}\left(1+\frac{3}{2}\gamma - \frac{3}{8}\gamma\frac{a^2}{s^2}\right) \tag{B3}$$

$$b' = \gamma\frac{a^5}{128s^7} \tag{B4}$$

$$s^2 = \frac{a^2}{4} - \frac{r_p^2}{6}$$

$$p = \frac{1}{4s^2}$$

where $r_p = 0.86$ fm is the radius of the proton. Nucleon-nucleus and nucleus-nucleus collisions are considered separately.

Nucleon-Nucleus

The matter density function for the nucleon is given by

$$\rho_P(\mathbf{x}-\mathbf{x}') = \delta(\mathbf{x}-\mathbf{x}') \tag{B5}$$

and for the target nucleus by

$$\rho_T(\mathbf{x}) = \rho_{TO}(a'_T + b'_T x^2)\exp(-px^2) \tag{B6}$$

The phase shift is given by equation (2),

$$\chi(b,e) = \frac{A_P^2 A_T^2}{k(A_P+A_T)}\int dz\int d^3\xi\rho_T(\boldsymbol{\xi})\int d^3y\rho_P(\mathbf{b}+z+\mathbf{y}+\boldsymbol{\xi})t(e,\mathbf{y})$$

Substituting for ρ_P, ρ_T, and $t(e,\mathbf{y})$ from equation (3), the integral is easily performed, obtaining

$$\chi_1(b,e) = 2\mathrm{Im}\chi(b,e) = f_1(e)f_2(b,e) \tag{B7}$$

where

$$f_1(e) = A_T\rho_{TO}\bar{\sigma}(e)\left[\frac{\pi}{P(e)}\right]^{1/2}\left[2B(e)(p+p')\right]^{-3/2} \tag{B8}$$

$$f_2(b,e) = (a_1 + a_2b^2)\exp[-P(e)b^2] \tag{B9}$$

with

$$a_1 = a' + 1.5\frac{b'}{p+p'} + \frac{a_2}{2P(e)}$$

$$a_2 = \frac{p'^2}{(p+p')^2} b'$$

$$p' = \frac{1}{2B(e)}$$

$$p = \frac{1}{4s_T^2}$$

$$P(e) = \frac{1}{4s_T^2 + 2B(e)} \tag{B10}$$

Also an expression for δ_2 in the Taylor expansion is derived as

$$\delta_2 = 2\left[\frac{\pi}{P(e)}\right]^{3/2} f_1(e)\left[a_1 + 1.5\frac{a_2}{P(e)} + a_2 R_e^2\right]\exp\left[-P(e)R_e^2\right] \tag{B11}$$

Nucleus-Nucleus

The matter density function for the projectile is

$$\rho_P(\mathbf{x}) = \rho_{PO}\left(a'_P + b'_P\, x^2\right)\exp(-px^2) \tag{B12}$$

and for the target is

$$\rho_T(\mathbf{x}) = \rho_{TO}(a'_T + b'_T\, x^2)\exp(-qx^2) \tag{B13}$$

which gives

$$\chi_1(b,e) = f_1(e) f_2(b,e) \tag{B14}$$

where

$$f_1(e) = A_P A_T\, \bar{\sigma}(e)\rho_{TO}\rho_{PO}\left\{2\pi B(e)[p+p'(e)][q+q'(e)]\right\}^{-3/2} \tag{B15}$$

and

$$f_2(b,e) = \left(a_1 + a_2\, b^2 + a_3\, b^4\right)\exp[-P(e)b^2] \tag{B16}$$

with

$$\left.\begin{aligned} p &= \frac{1}{4s_P^2} \\ q &= \frac{1}{4s_T^2} \\ q' &= \frac{1}{2B(e)} \\ p'(e) &= \left[4s_T^2 + 2B(e)\right]^{-1} \\ P(e) &= \left[4\left(s_P^2 + s_T^2\right) + 2B(e)\right]^{-1} \end{aligned}\right\} \tag{B17}$$

$$a_1 = a'_P a''_T + \frac{1.5}{p+p'}\left(a''_T b'_P + a'_P b'_T\right) + \frac{15}{4}\,\frac{b'_T b'_P}{(p+p')^2}$$

$$a_2 = a''_T b'_P \frac{p'^2}{(p+p')^2} + a'_P b'_T \frac{p^2}{(p+p')^2} - b'_T b'_P 2\frac{pp'}{(p+p')^3} + b'_T b'_P \frac{3}{2}\,\frac{p^2+p'^2}{(p+p')^3}$$

$$a_3 = b'_T b'_P \frac{p^2 p'^2}{(p+p')^4}$$

where a'_P and b'_P are the constants that relate to the projectile as given by equations (B3) and (B4) and

$$a'_T = \frac{a_T^3}{8s_T^3}\left[\left(1 + \frac{3}{2}\gamma_T - \frac{3\gamma_T a_T^2}{8s_T^2}\right) + \frac{\gamma_T a_T^2}{16 s_T^4}\,\frac{1.5}{(q+q')}\right]$$

$$b'_T = \frac{a_T^3}{8s_T^3}\,\frac{\gamma_T a_T^2}{16 s_T^4}\left[\frac{q'^2}{(q+q')^2}\right]$$

$$a''_T = a'_T + b'_T \frac{1.5}{q+q'}$$

relate to the targets.

An expression for δ_2 in the Taylor series expansion is derived as

$$\delta_2 \approx \frac{f_1(e)}{2P(e)}\sqrt{\frac{\pi}{P(e)}}\left\{a_1 + a_2\left[\frac{1.5}{P(e)} + R_e^2\right] + a_3\left[\frac{15}{4P(e)^2} + \frac{3R_e^2}{P(e)} + 4R_e^4\right]\right\}\exp\left[-P(e)R_e^2\right] \tag{B18}$$

The following integral relations were used.

$$I = \int_{-\infty}^{\infty} \exp[-qr^2 - p(\mathbf{r}-\mathbf{y})^2]\,d\mathbf{r} = \left(\frac{\pi}{q+p}\right)^{3/2}\exp\left(-\frac{pq}{p+q}\right)y^2 \tag{B19}$$

$$\int r^2 \exp[-qr^2 - p(\mathbf{r}-\mathbf{y})^2]\,d\mathbf{r} = -\frac{\partial}{\partial q}I \tag{B20}$$

$$\int (\mathbf{r}-\mathbf{y})^2 \exp[-qr^2 - p(\mathbf{r}-\mathbf{y})^2]\,d\mathbf{r} = -\frac{\partial}{\partial p}I \tag{B21}$$

$$\int r^2(\mathbf{r}-\mathbf{y})^2 \exp[-qr^2 - p(\mathbf{r}-\mathbf{y})^2]\,d\mathbf{r} = \left(-\frac{\partial}{\partial p}\right)\left(-\frac{\partial}{\partial q}\right)I \tag{B22}$$

An alternate partial evaluation is given in reference 30.

Appendix C

Parameterization for Experimental Two-Nucleon Total Cross Section

For completeness, the isospin-averaged nucleon-nucleon cross section taken from reference 1 is given. A parameterization for the experimental two-nucleon total cross section in millibarns (1 barn = 1×10^{-28} m^2) is given for the proton-proton interaction by

$$\sigma_{pp}(e) = \left(1 + \frac{5}{e}\right)\left\{40 + 109\cos\left(0.199\sqrt{e}\right)\exp\left[-0.451(e-25)^{0.258}\right]\right\} \tag{C1}$$

for $e \geq 25$ MeV and for the lower energies by

$$\sigma_{pp}(e) = \exp\left\{6.51\exp\left[-\left(\frac{e}{134}\right)^{0.7}\right]\right\} \tag{C2}$$

For proton-neutron interaction at $e \geq 0.1$ MeV,

$$\sigma_{np}(e) = 38 + 12\,500\exp\left[-1.187(e-0.1)^{0.35}\right] \tag{C3}$$

and at lower energies

$$\sigma_{np}(e) = 26\,000\exp\left[-\left(\frac{e}{0.282}\right)^{0.3}\right] \tag{C4}$$

The isospin average is calculated as follows:

$$\bar{\sigma}(e) = \left[\left(N_P N_T + Z_P Z_T\right)\sigma_{pp} + \left(N_P Z_T + Z_P N_T\right)\sigma_{np}\right]/A_P A_T \tag{C5}$$

where A, N, and Z are the atomic, neutron, and proton numbers, respectively.

The nucleon-nucleon slope parameter is parameterized (ref. 31) as

$$B(e) = 10 + 0.5\ln\left(\frac{s'}{s_o}\right) \tag{C6}$$

where s' is the square of the nucleon-nucleon center-of-mass energy and $s_o = (1\ \text{GeV}/c)^{-2}$.

References

1. Wilson, John W.; Townsend, Lawrence W.; Schimmerling, Walter; Khandelwal, Govind S.; Khan, Ferdous; Nealy, John E.; Cucinotta, Francis A.; Simonsen, Lisa C.; Shinn, Judy L.; and Norbury, John W.: *Transport Methods and Interactions for Space Radiations*. NASA RP-1257, 1991.

2. Glauber, R. J.: High-Energy Collision Theory. *Lectures in Theoretical Physics, Volume I*, Wesley E. Brittin and Lita G. Dunham, eds., Interscience Publ., Inc., 1959, pp. 315–414.

3. Joachain, Charles J.: *Quantum Collision Theory*, Third ed. Elsevier Science Publ. Co. Inc., 1983.

4. Kerman, A. K.; McManus, H.; and Thaler, R. M.: The Scattering of Fast Nucleons From Nuclei. *Ann. Phys. (N.Y.)*, vol. 8, no. 4, Dec. 1959, pp. 551–635.

5. Wilson, John W.: Composite Particle Reaction Theory. Ph.D. Diss., College of William and Mary in Virginia, June 1975.

6. Wilson, J. W.; and Townsend, L. W.: An Optical Model for Composite Nuclear Scattering. *Canadian J. Phys.*, vol. 59, no. 11, 1981, pp. 1569–1576.

7. Karol, Paul J.: Nucleus-Nucleus Reaction Cross Sections at High Energies: Soft-Spheres Model. *Phys. Review C*, vol. 11, no. 4, Apr. 1975, pp. 1203–1209.

8. Charagi, S. K.; and Gupta, S. K.: Coulomb-Modified Glauber Model Description of Heavy-Ion Reaction Cross Sections. *Phys. Review C*, vol. 41, no. 4, Apr. 1990, pp. 1610–1618.

9. Ernst, David J.: Total Reaction Cross Sections and the Matter Density of Finite Nuclei. *Phys. Review C*, vol. 19, no. 3, Mar. 1979, pp. 896–904.

10. DiGiacomo, N. J.; DeVries, R. M.; and Peng, J. C.: Microscopic Description of Nucleon-Nucleus Total Reaction Cross Sections. *Phys. Review Lett.*, vol. 45, no. 7, Aug. 18, 1980, pp. 527–531.

11. DeVries, R. M.; and Peng, J. C.: Nucleus-Nucleus Total Reaction Cross Sections. *Phys. Review C*, vol. 22, no. 3, Sept. 1980, pp. 1055–1064.

12. Townsend, L. W.; and Wilson, J. W.: Comment on "Nucleus-Nucleus Total Reaction Cross Sections." *Phys. Review*, ser. C, vol. 25, no. 3, Mar. 1982, pp. 1679–1681.

13. Bradt, H. L.; and Peters, B.: The Heavy Nuclei of the Primary Cosmic Radiation. *Phys. Review*, second ser., vol. 77, no. 1, Jan. 1, 1950, pp. 54–70.

14. Townsend, L. W.; Wilson, J. W.; and Bidasaria, H. B.: On the Geometric Nature of High-Energy Nucleus-Nucleus Reaction Cross Sections. *Canadian J. Phys.*, vol. 60, no. 10, Oct. 1982, pp. 1514–1518.

15. Townsend, L. W.; and Wilson, J. W.: Energy-Dependent Parameterization of Heavy-Ion Absorption Cross Sections. *Radiat. Res.*, vol. 106, 1986, pp. 283–287.

16. Townsend, L. W.; and Wilson, J. W.: Comment on "Trends of Total Reaction Cross Sections for Heavy Ion Collisions in the Intermediate Energy Range." *Phys. Review C*, vol. 37, no. 2, Feb. 1988, pp. 892–893.

17. Shen, Wen-Qing; Wang, Bing; Feng, Jun; Zhan, Wen-Long; Zhu, Yong-Tai; and Feng, En-Pu: Total Reaction Cross Section for Heavy-Ion Collisions and Its Relation to the Neutron Excess Degree of Freedom. *Nucl. Phys.*, vol. A491, 1989, pp. 130–146.

18. Vitturi, A.; and Zardi, F.: Modified Glauber Model for the Description of Elastic Scattering Between Heavy Ions. *Phys. Review C*, vol. 36, no. 4, Oct. 1987, pp. 1404–1407.

19. Hussein, M. S.; Rego, R. A.; and Bertulani, C. A.: Microscopic Theory of the Total Reaction Cross Section and Application to Stable and Exotic Nuclei. *Phys. Lett.*, vol. 201, no. 5, 1991, pp. 279–334.

20. Menet, J. J. H.; Gross, E. E.; Malanify, J. J.; and Zucker, A.: Total-Reaction-Cross-Section Measurements for 30–60-MeV Protons and the Imaginary Optical Potential. *Phys. Review C*, vol. 4, no. 4, Oct. 1971, pp. 1114–1129.

21. Barashenkov, V. S.; Gudima, K. K.; and Toneev, V. D.: Cross Sections for Fast Particles and Atomic Nuclei. *Prog. Phys.*, vol. 17, no. 10, 1969, pp. 683–725.

22. Renberg, P. U.; Measday, D. F.; Pepin, M.; Schwaller, P.; Favier, B.; and Richard-Serre, C.: Reaction Cross Sections for Protons in the Energy Range 220–570 MeV. *Nucl. Phys.*, vol. A183, no. 1, Mar. 20, 1972, pp. 81–104.

23. Perrin, C.; Kox, S.; Longequeue, N.; Viano, J. B.; Buenerd, M.; Cherkaoui, R.; Cole, A. J.; Gamp, A.; Menet, J.; Ost, R.; Bertholet, R.; Guet, C.; and Pinston, J.: Direct Measurement of the $^{12}C + {}^{12}C$ Reaction Cross Section Between 10 and 83 MeV/Nucleon. *Phys. Review Lett.*, vol. 49, no. 26, Dec. 27, 1982, pp. 1905–1909.

24. Buenerd, M.; Lounis, A.; Chauvin, J.; Lebrun, D.; Martin, P.; Duhamel, G.; Gondrand, J. C.; and De Saintignon, P.: Elastic and Inelastic Scattering of Carbon Ions at Intermediate Energies. *Nucl. Phys.*, vol. A424, no. 2, Aug. 6, 1984, pp. 313–334.

25. Kox, S.; Gamp, A.; Perrin, C.; Arvieux, J.; Bertholet, R.; Bruandet, J. F.; Buenerd, M.; Cherkaoui, R.; Cole, A. J.; El-Masri, Y.; Longequeue, N.; Menet, J.; Merchez, F.; and Viano, J. B.: Trends of Total Reaction Cross Sections for Heavy Ion Collisions in the Intermediate Energy Range. *Phys. Review C*, vol. 35, no. 5, May 1987, pp. 1678–1691.

26. Dubar, L. V.; Eleukenov, D. Sh.; Slyusarenko, L. I.; and Yurkuts, N. P.: Parametrization of Total Cross Sections of Reactions in the Intermediate Energy Region. *Sov. J. Nucl. Phys.*, vol. 49, no. 5, May 1989, pp. 771–773.

27. De Vries, H.; De Jager, C. W.; and De Vries, C.: Nuclear Charge-Density-Distribution Parameters From Elastic Electron Scattering. *At. Data & Nucl. Data Tables*, no. 36, 1987, pp. 495–536.

28. Bender, Carl M.; and Orszag, Steven A.: *Advanced Mathematical Methods for Scientists and Engineers*. McGraw-Hill Book Co., c.1978.

29. Townsend, Lawrence W.: *Harmonic Well Matter Densities and Pauli Correlation Effects in Heavy-Ion Collisions*. NASA TP-2003, 1982.

30. Bidasaria, Hari B.; and Townsend, Lawrence W.: *Analytic Optical Potentials for Nucleon-Nucleus and Nucleus-Nucleus Collisions Involving Light and Medium Nuclei*. NASA TM-83224, 1982.

31. Ringia, F. E.; Dobrowolski, T.; Gustafson, H. R.; Jones, L. W.; Longo, M. J.; Parker, E. F.; and Cork, Bruce: Differential Cross Sections for Small-Angle Neutron-Proton and Neutron-Nucleus Elastic Scattering at 4.8 GeV/c. *Phys. Review Lett.*, vol. 28, no. 3, Jan. 17, 1972, pp. 185–188.

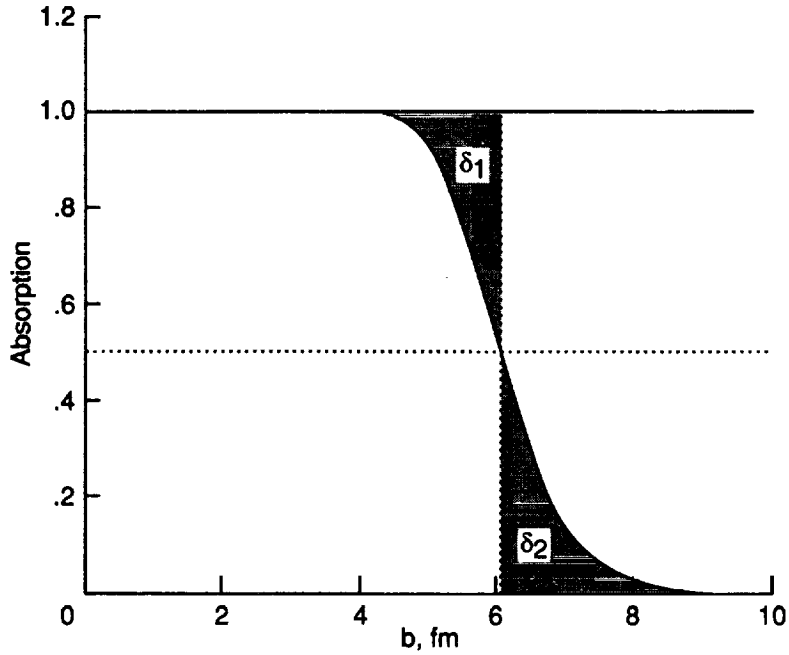

Figure 1. Absorption as a function of impact parameter for nuclear collisions. At half absorption, shaded areas $\delta_1 \approx \delta_2$.

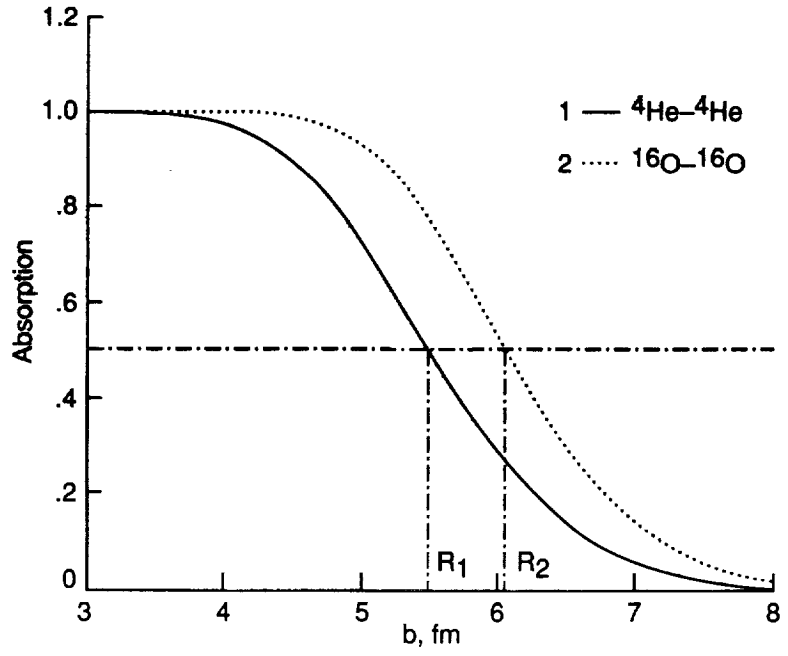

Figure 2. Absorption as a function of impact parameter for projectile-target systems of ^{4}He–^{4}He and ^{16}O–^{16}O at 2 GeV/nucleon. Terms R_1 and R_2 denote geometric radii for systems.

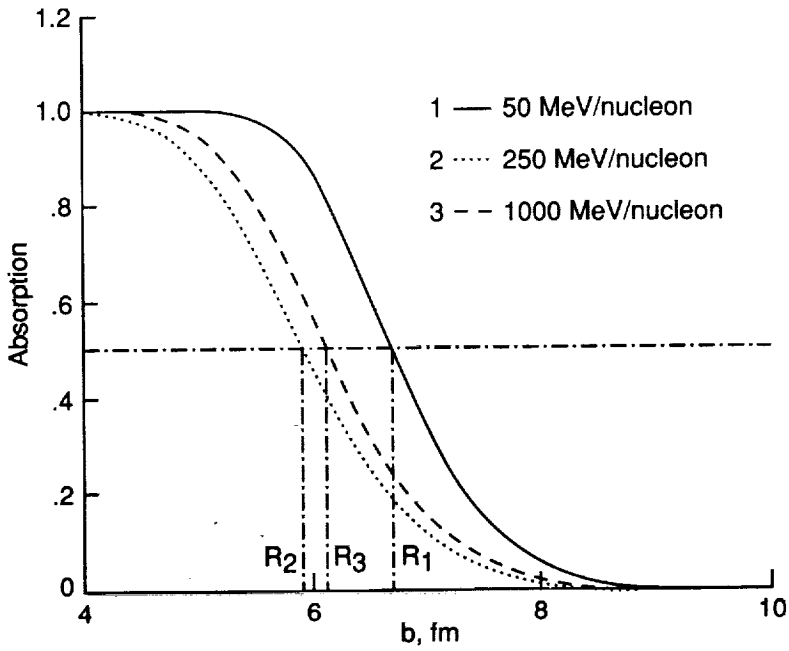

Figure 3. Absorption as a function of impact parameter for three energy values: 50 and 250 MeV/nucleon and 1 GeV/nucleon. Corresponding effective radii R_1, R_2, and R_3 are indicated.

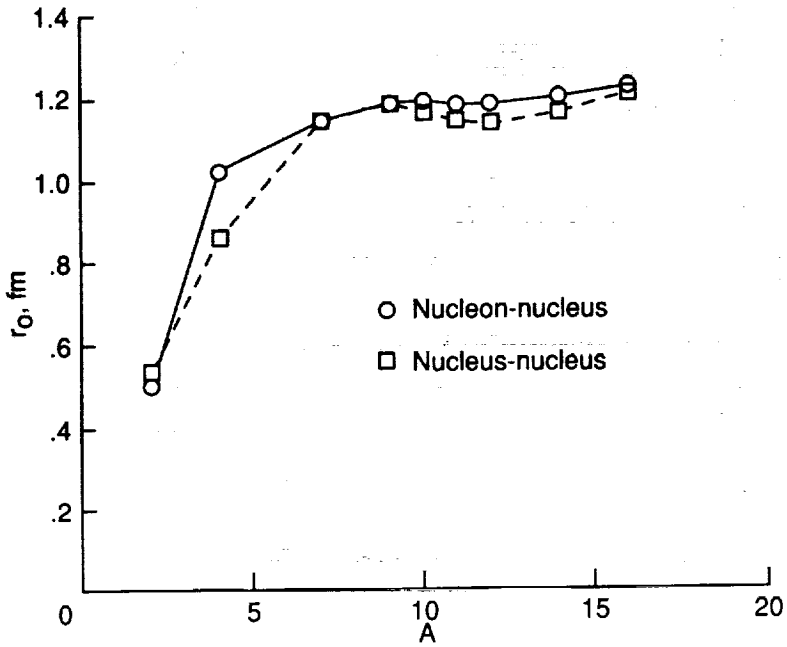

Figure 4. Variation of r_o with atomic mass for harmonic oscillator density functions for nucleon-nucleus and identical nucleus-nucleus collisions.

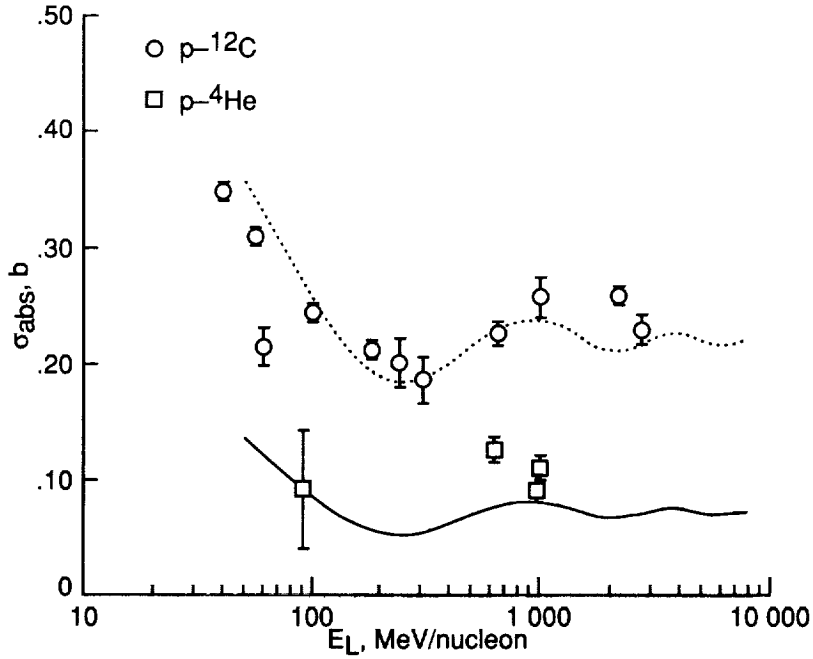

Figure 5. Variation of absorption cross section with energy for proton-nucleus collisions.

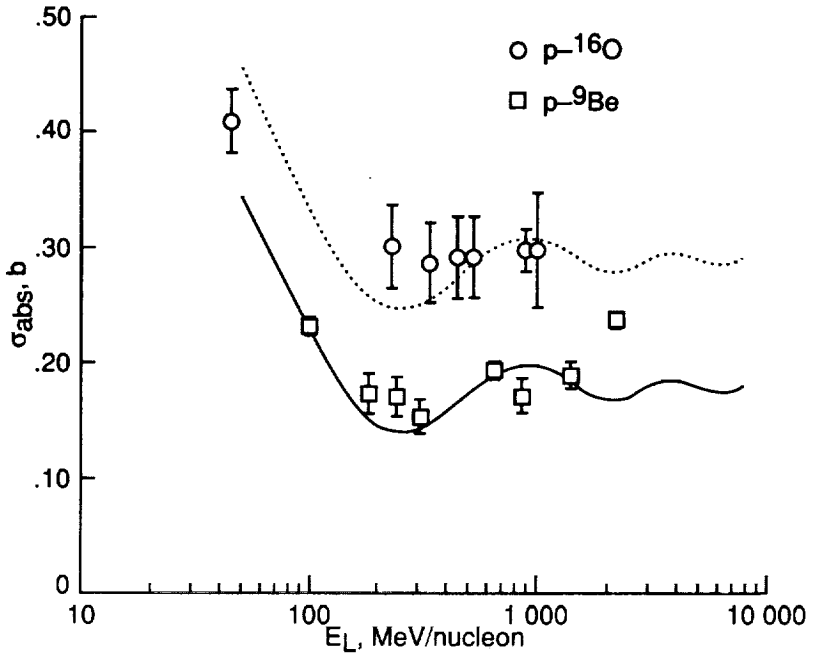

Figure 6. Variation of absorption cross section with energy for proton-nucleus collisions.

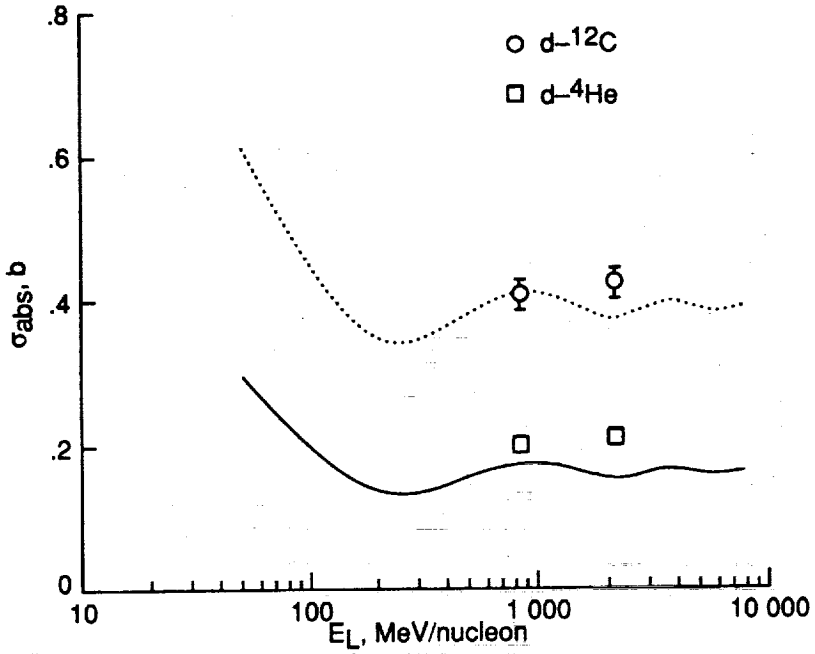

Figure 7. Variation of absorption cross section with energy for deuteron-nucleus collisions.

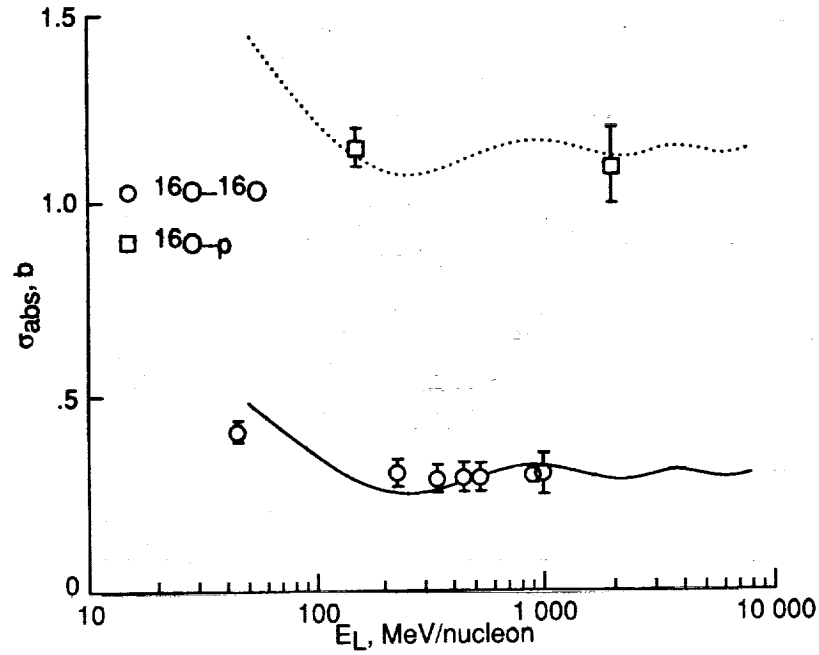

Figure 8. Variation of absorption cross section with energy for oxygen-nucleus systems.

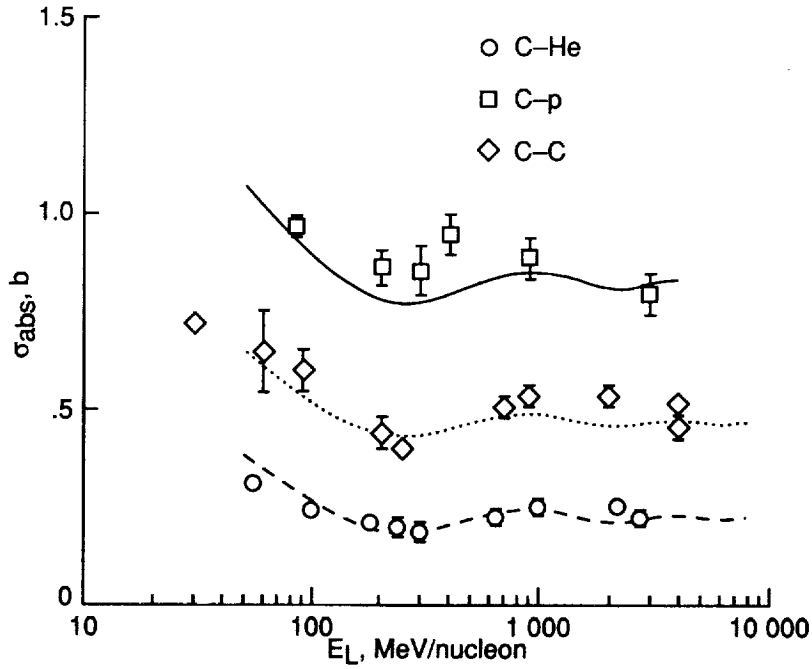

Figure 9. Variation of absorption cross section with energy for carbon-nucleus systems.

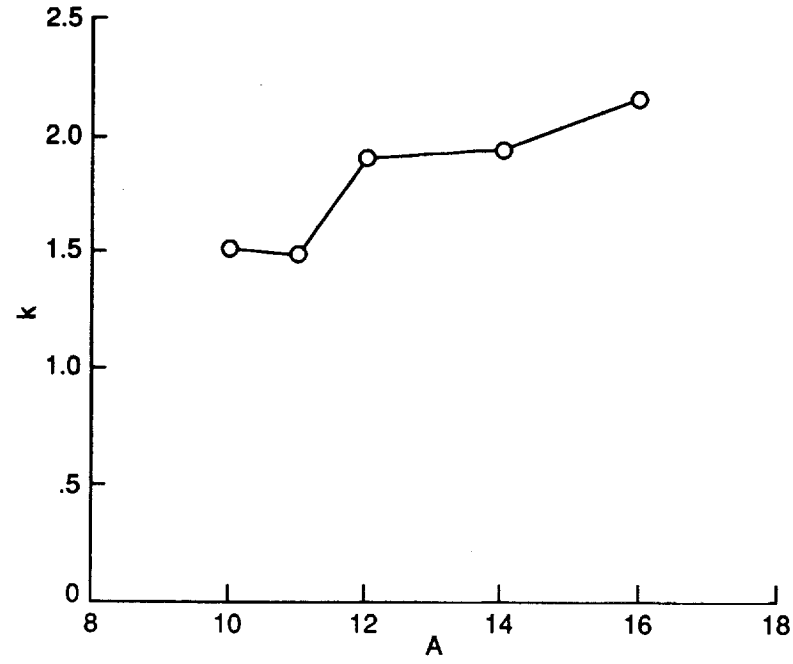

Figure 10. Variation of $k = (R/a)^2$ for harmonic oscillator functions with atomic mass number, where R is half-density radius and a fm is harmonic oscillator parameter.

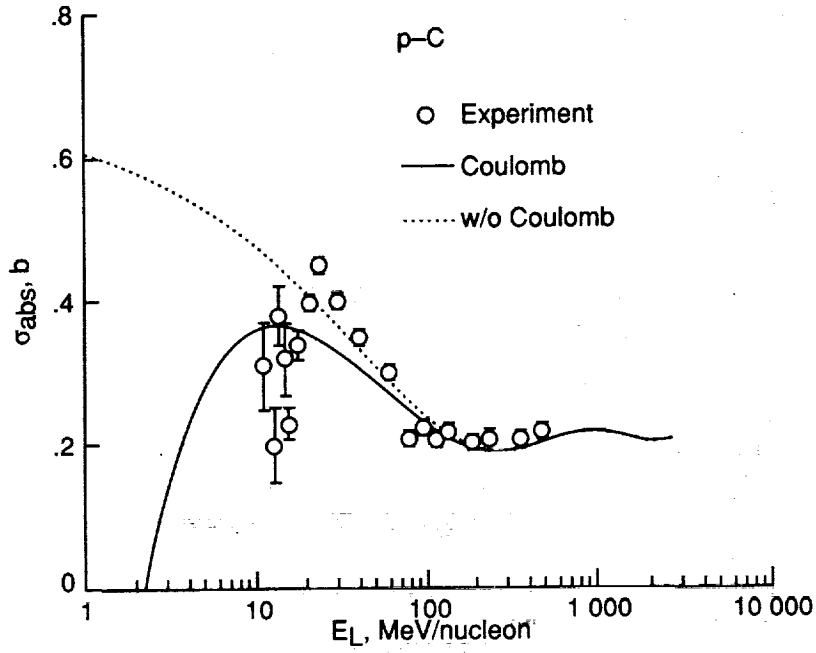

Figure 11. Absorption cross section as a function of energy for proton on carbon with and without Coulomb effects.

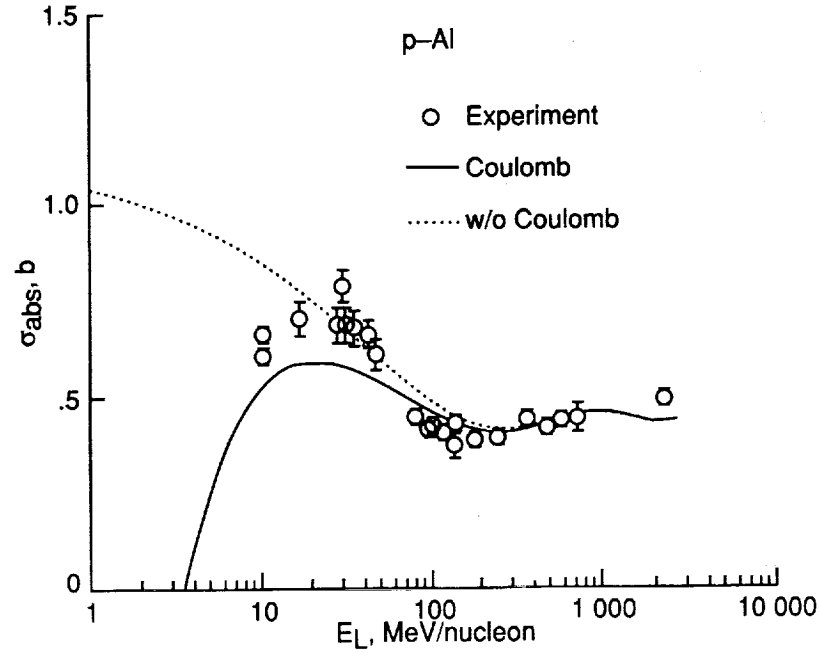

Figure 12. Absorption cross section as a function of energy for proton on aluminum with and without Coulomb effects.

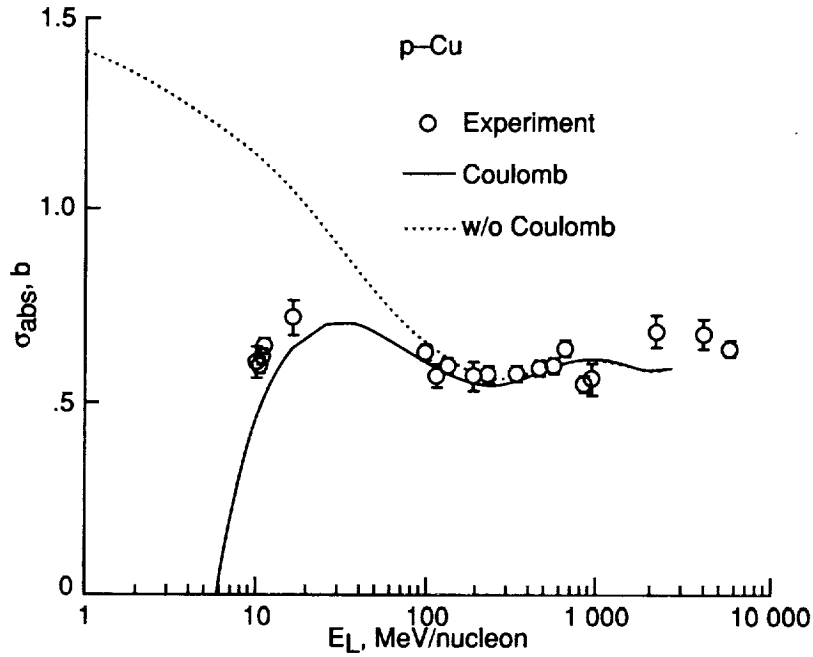

Figure 13. Absorption cross section as a function of energy for proton on copper with and without Coulomb effects.

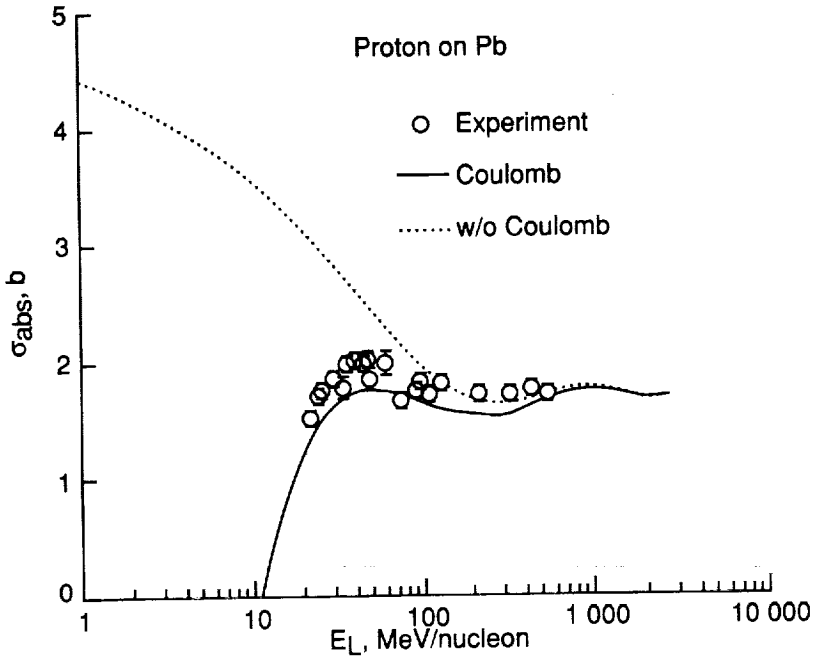

(a) Proton on lead.

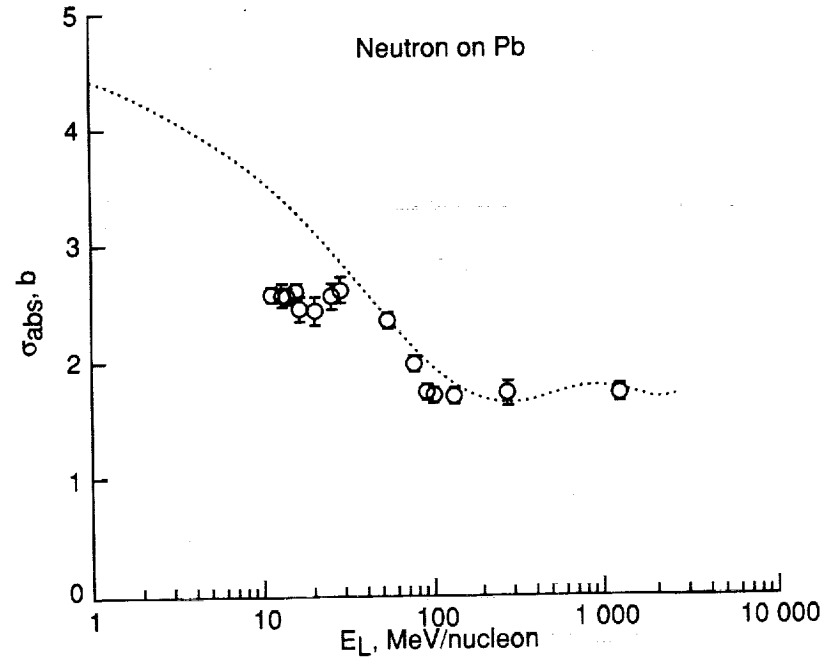

(b) Neutron on lead.

Figure 14. Absorption cross section for proton or neutron on lead as a function of energy with and without Coulomb effects. Without Coulomb effects, curve corresponds to neutron projectiles.

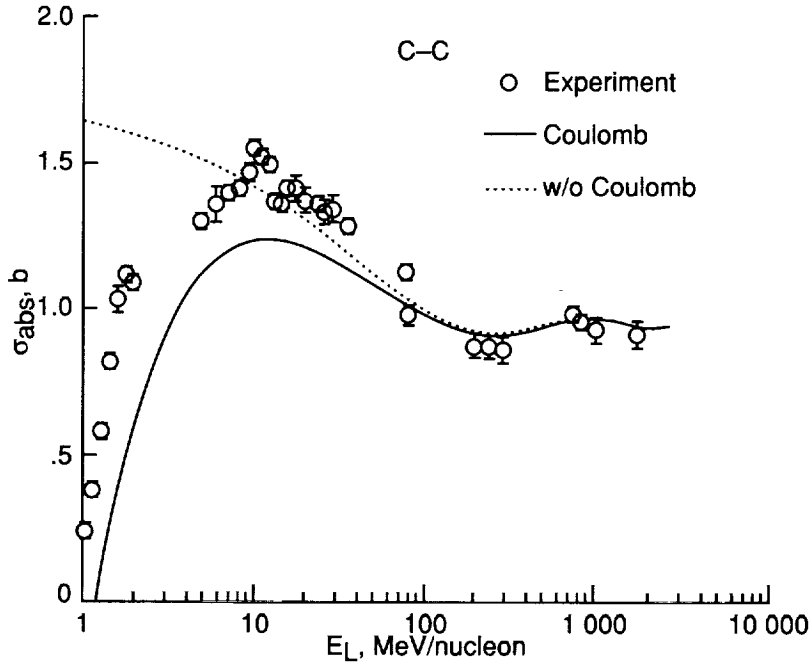

Figure 15. Absorption cross section as a function of energy for carbon on carbon with and without Coulomb effects.

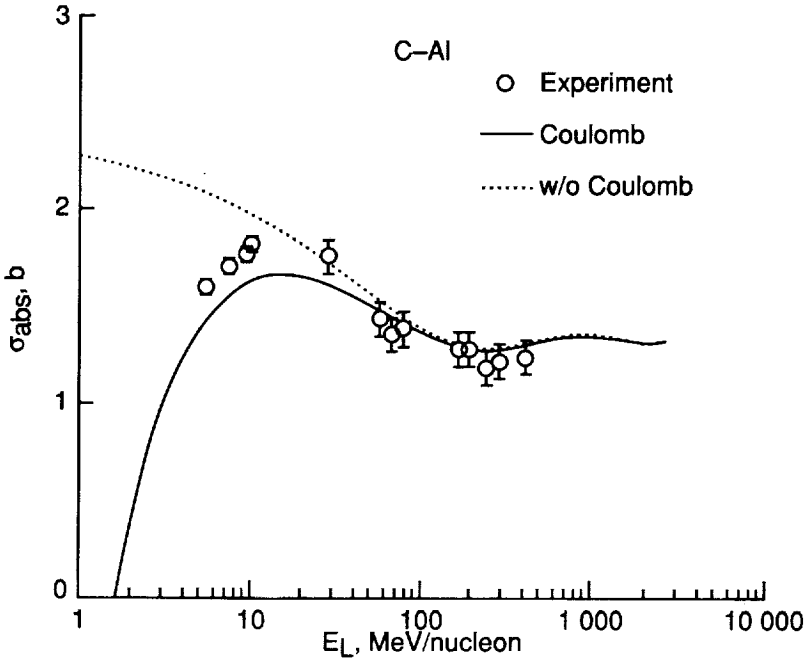

Figure 16. Absorption cross section as a function of energy for carbon on aluminum with and without Coulomb effects.

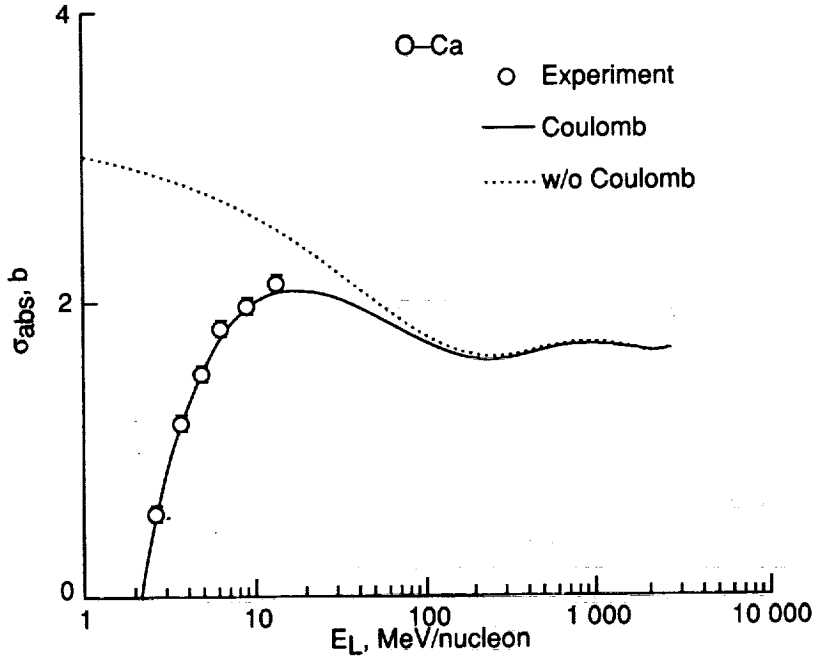

Figure 17. Absorption cross section as a function of energy for oxygen on calcium with and without Coulomb effects.

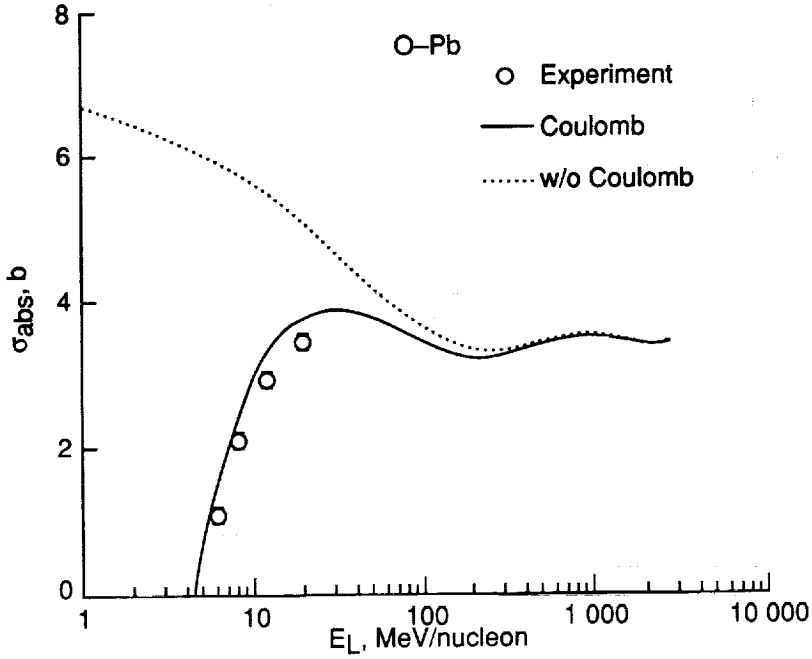

Figure 18. Absorption cross section as a function of energy for oxygen on lead with and without Coulomb effects.

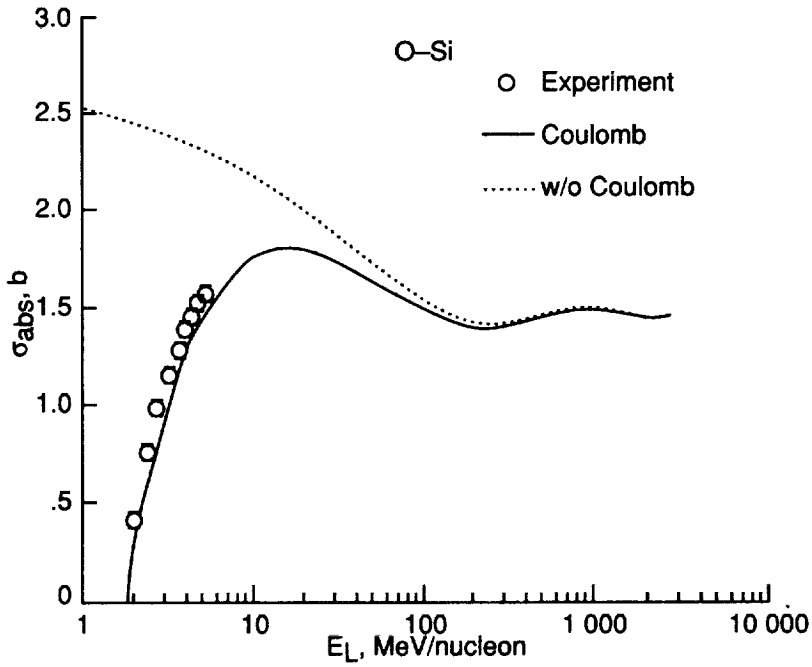

Figure 19. Absorption cross section as a function of energy for oxygen on silicon with and without Coulomb effects.

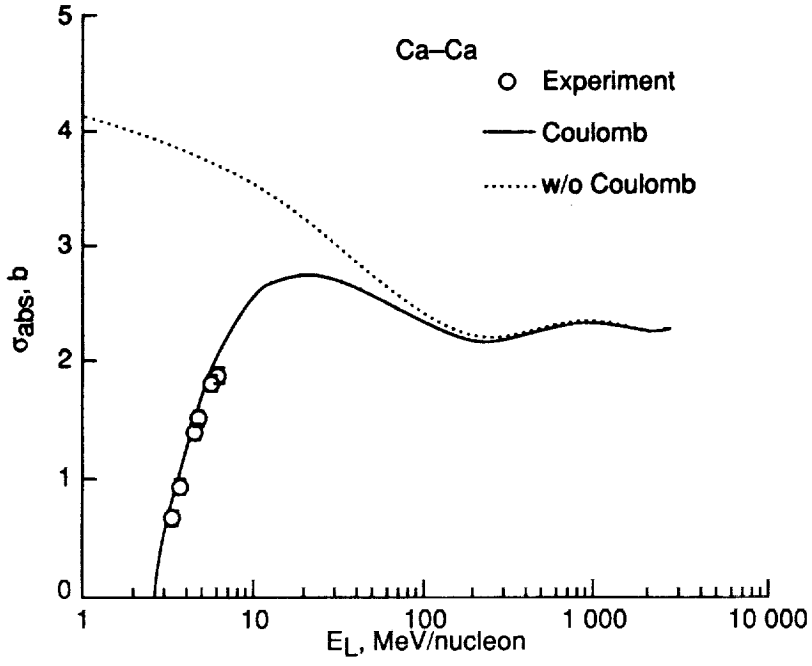

Figure 20. Absorption cross section as a function of energy for calcium on calcium with and without Coulomb effects.

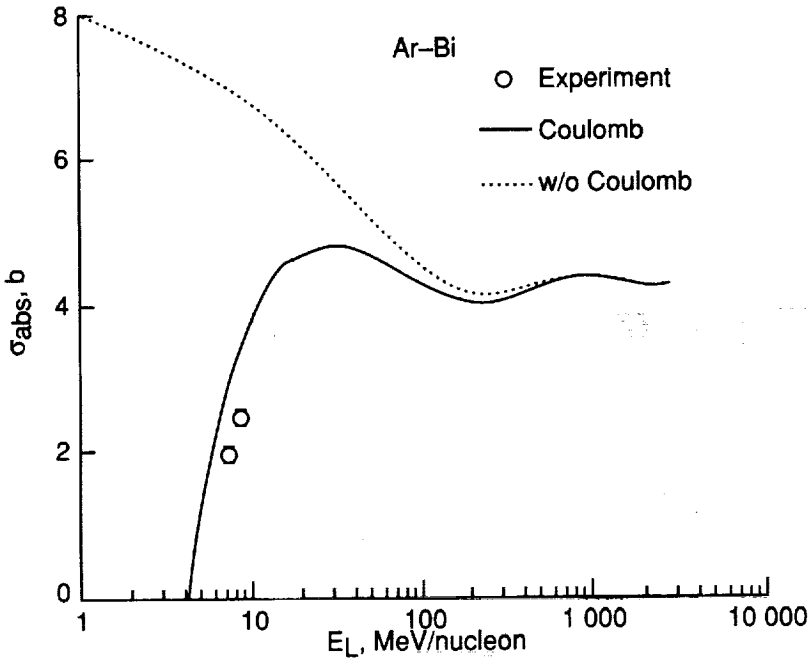

Figure 21. Absorption cross section as a function of energy for argon on bismuth with and without Coulomb effects.

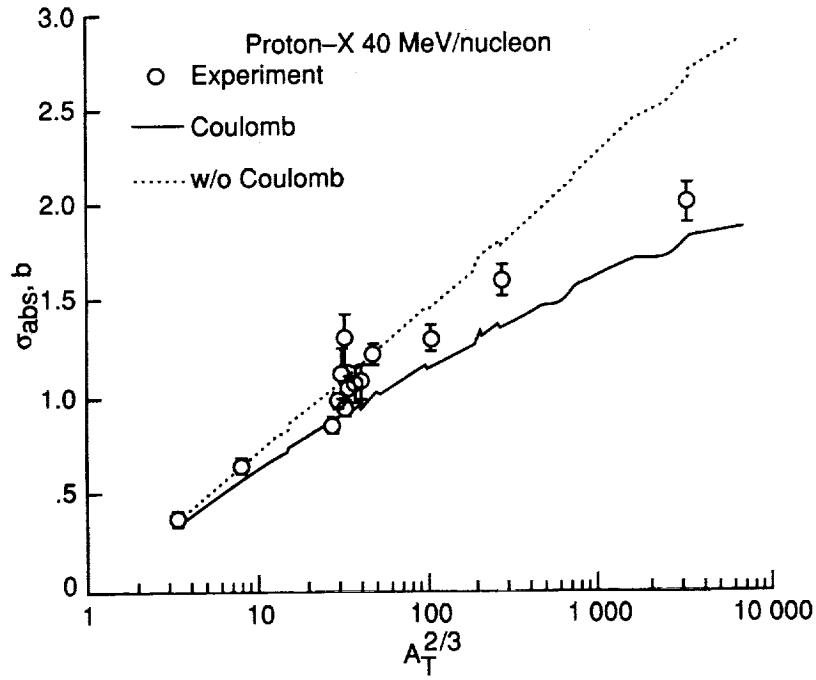

Figure 22. Absorption cross section as a function of $\left(A_T^{2/3}\right)$ for protons on targets at 40 MeV/nucleon with and without Coulomb effects, where A_T is target mass number.

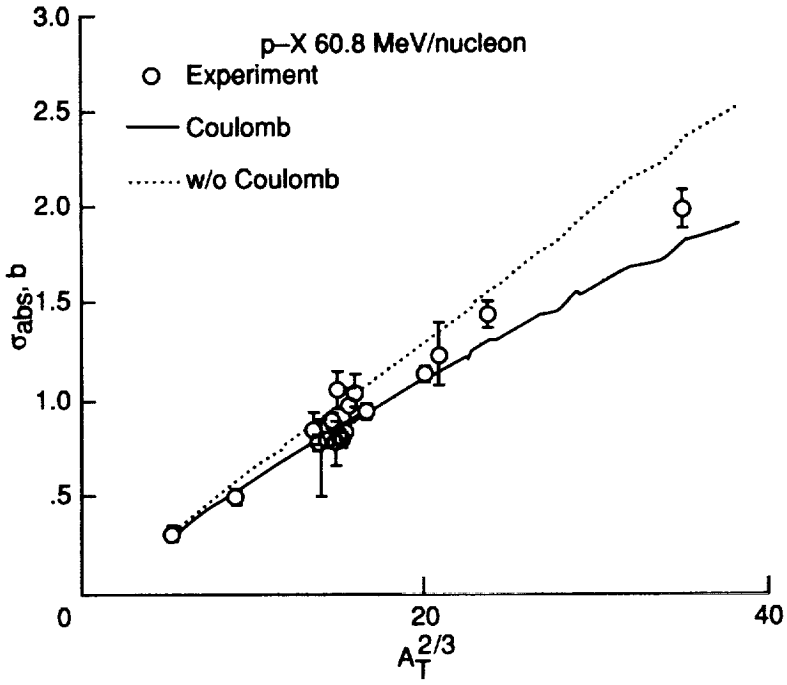

Figure 23. Absorption cross section as a function of $\left(A_T^{1/3}\right)^2$ for protons on targets at 60.8 MeV/nucleon with and without Coulomb effects, where A_T is target mass number.

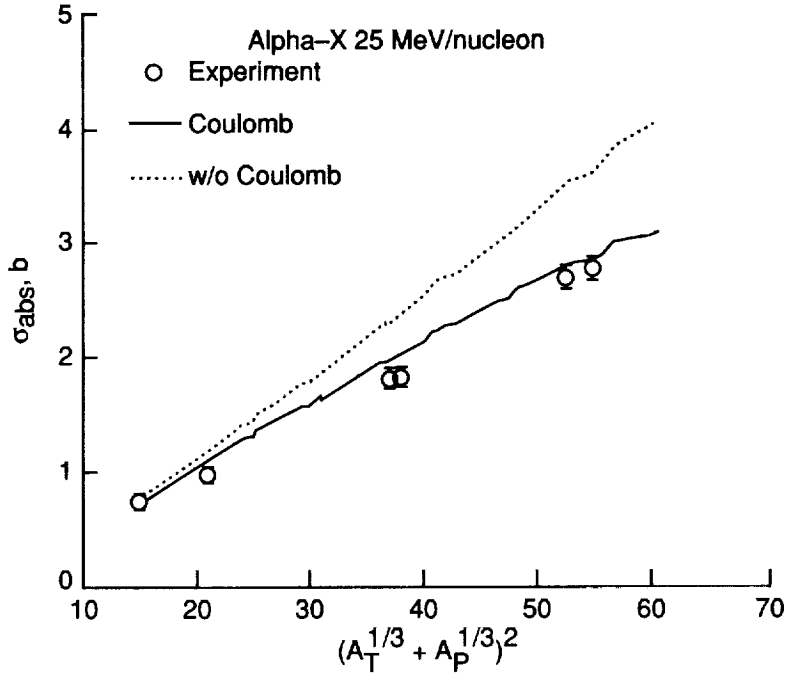

Figure 24. Absorption cross section as a function of $\left(A_T^{1/3} + A_P^{1/3}\right)^2$ for alpha particles on targets at 25 MeV/nucleon with and without Coulomb effects, where A_P is mass number of alpha particles and A_T is target mass number.

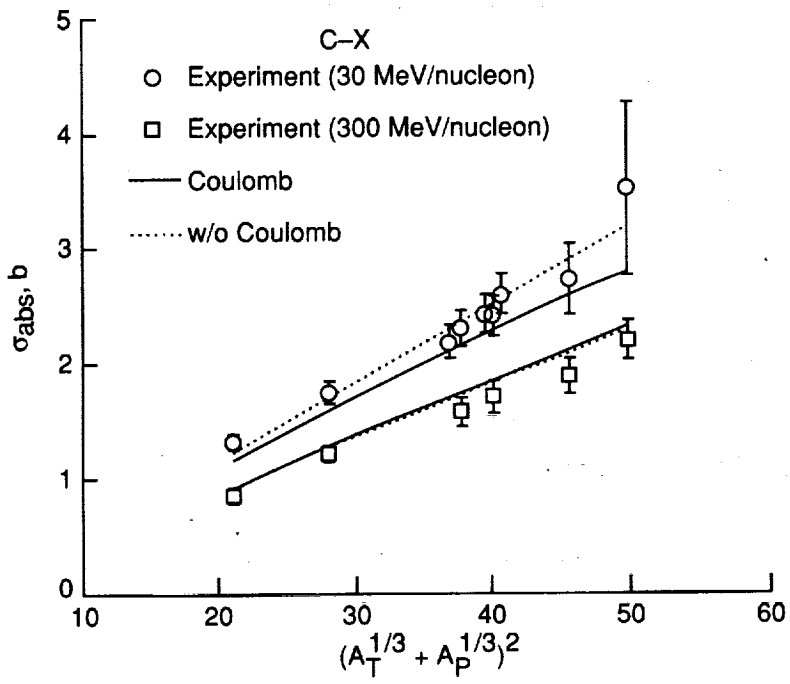

Figure 25. Absorption cross section as a function of $\left(A_T^{1/3} + A_P^{1/3}\right)^2$ for carbon on targets at 30 MeV/nucleon and 300 MeV/nucleon with and without Coulomb effects.

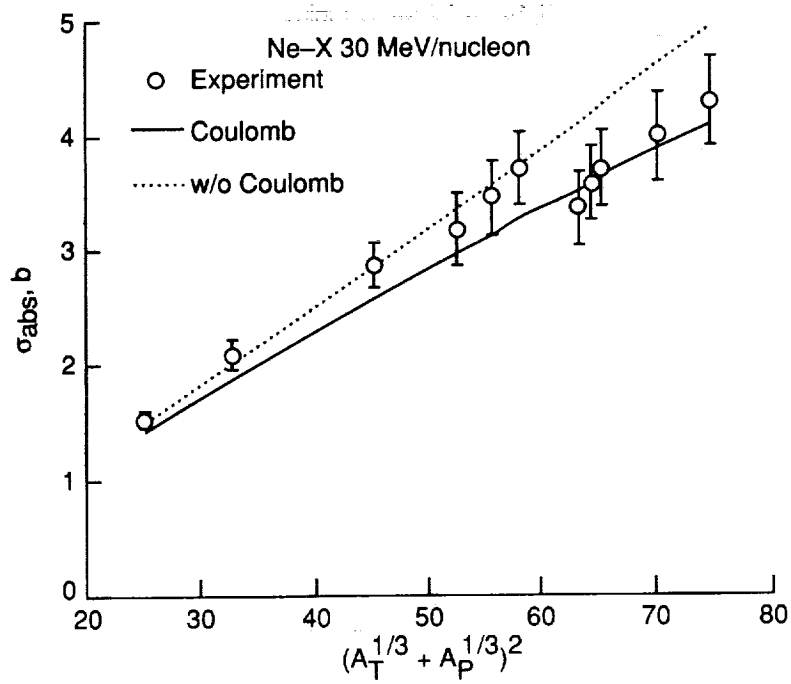

Figure 26. Absorption cross section as a function of $\left(A_T^{1/3} + A_P^{1/3}\right)^2$ for neon on targets at 30 MeV/nucleon with and without Coulomb effects.

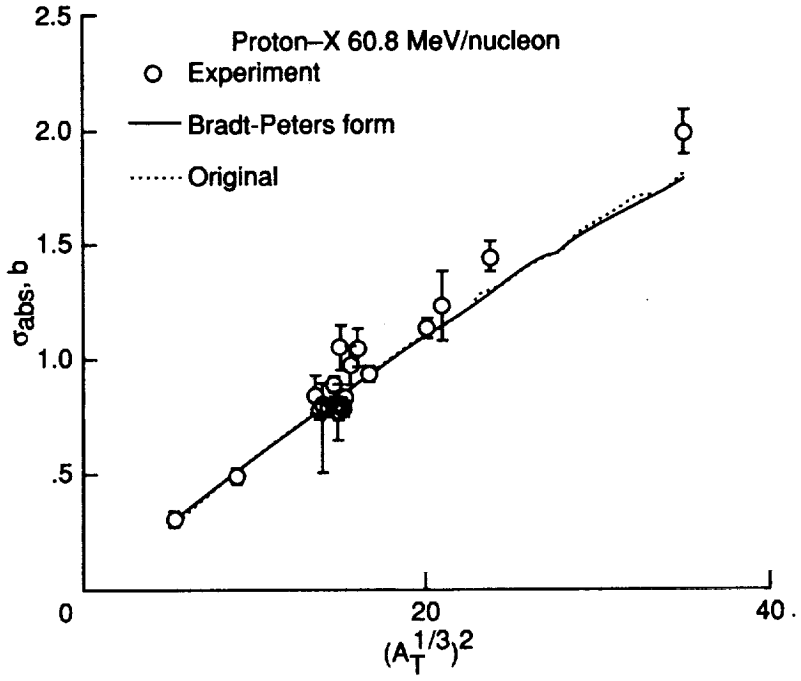

Figure 27. Comparison of Bradt-Peters form with that for absorption cross section of proton on targets at 60.8 MeV/nucleon.

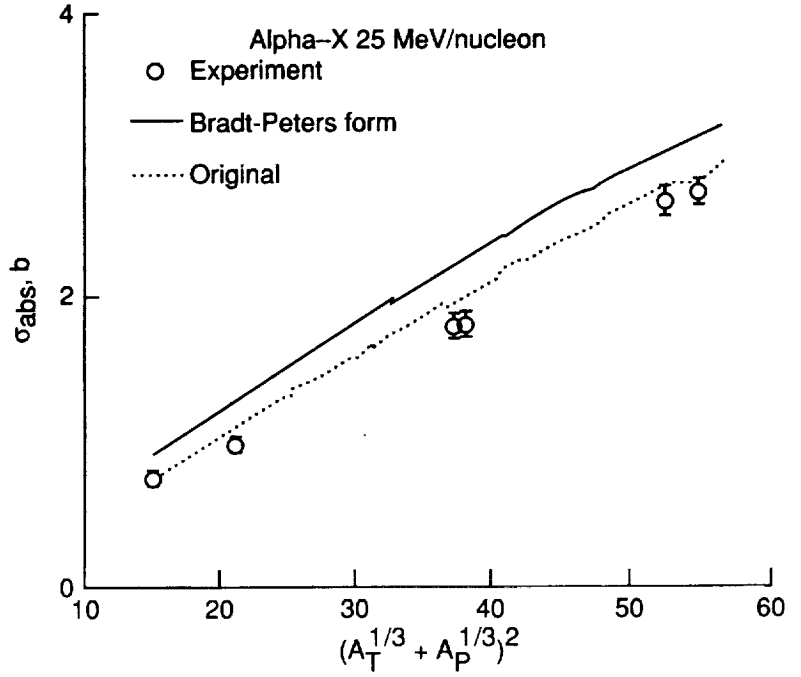

Figure 28. Comparison of Bradt-Peters form with that for alpha on targets at 25 MeV/nucleon.

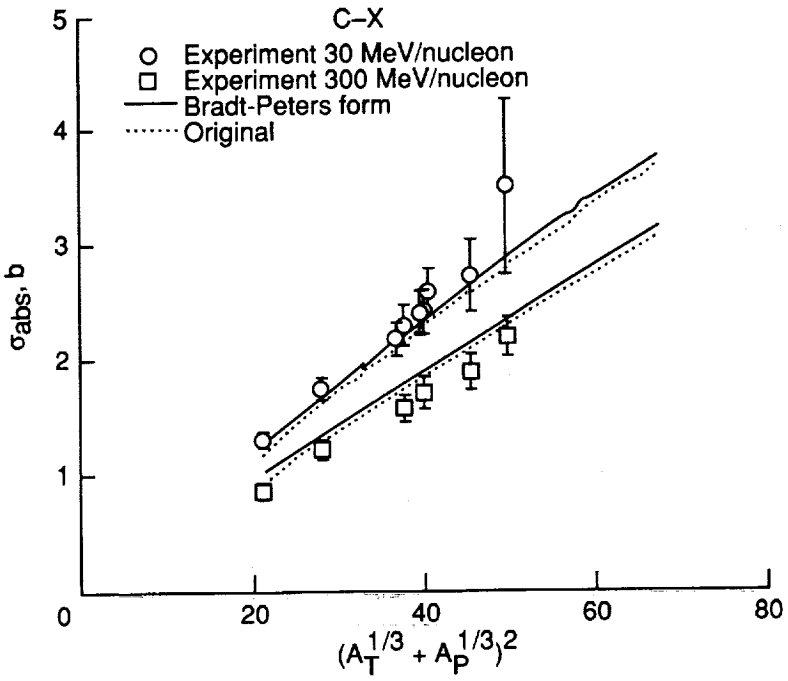

Figure 29. Comparison of Bradt-Peters form with that for carbon on targets at 30 MeV/nucleon and 300 MeV/nucleon.

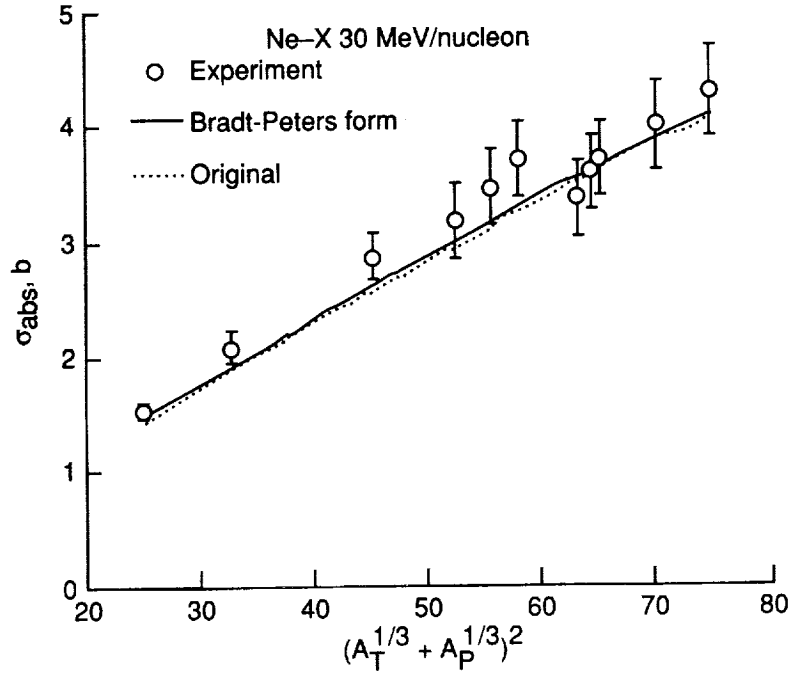

Figure 30. Comparison of Bradt-Peters form with that for neon on targets at 30 MeV/nucleon.

REPORT DOCUMENTATION PAGE

Form Approved
OMB No. 0704-0188

1. AGENCY USE ONLY *(Leave blank)*	2. REPORT DATE	3. REPORT TYPE AND DATES COVERED
	July 1993	Technical Paper

4. TITLE AND SUBTITLE
Geometric Model From Microscopic Theory for Nuclear Absorption

5. FUNDING NUMBERS
WU 593-42-21-01

6. AUTHOR(S)
Sarah John, Lawrence W. Townsend, John W. Wilson,
and Ram K. Tripathi

7. PERFORMING ORGANIZATION NAME(S) AND ADDRESS(ES)
NASA Langley Research Center
Hampton, VA 23681-0001

8. PERFORMING ORGANIZATION REPORT NUMBER
L-17187

9. SPONSORING/MONITORING AGENCY NAME(S) AND ADDRESS(ES)
National Aeronautics and Space Administration
Washington, DC 20546-0001

10. SPONSORING/MONITORING AGENCY REPORT NUMBER
NASA TP-3324

11. SUPPLEMENTARY NOTES
John and Tripathi: ViGYAN, Inc., Hampton VA; Townsend and Wilson: Langley Research Center, Hampton, VA.

12a. DISTRIBUTION/AVAILABILITY STATEMENT
Unclassified–Unlimited

Subject Category 73

12b. DISTRIBUTION CODE

13. ABSTRACT *(Maximum 200 words)*
A parameter-free geometric model for nuclear absorption is derived herein from microscopic theory. The expression for the absorption cross section in the eikonal approximation, taken in integral form, is separated into a geometric contribution that is described by an energy-dependent effective radius and two surface terms that cancel in an asymptotic series expansion. For collisions of light nuclei, an expression for the effective radius is derived from harmonic oscillator nuclear density functions. A direct extension to heavy nuclei with Woods-Saxon densities is made by identifying the equivalent half-density radius for the harmonic oscillator functions. Coulomb corrections are incorporated, and a simplified geometric form of the Bradt-Peters type is obtained. Results spanning the energy range from 1 MeV/nucleon to 1 GeV/nucleon are presented. Good agreement with experimental results is obtained.

14. SUBJECT TERMS	15. NUMBER OF PAGES
Reaction cross section; Nuclear scattering; Bradt-Peters formula; Spacecraft shielding	31
	16. PRICE CODE A03

17. SECURITY CLASSIFICATION OF REPORT	18. SECURITY CLASSIFICATION OF THIS PAGE	19. SECURITY CLASSIFICATION OF ABSTRACT	20. LIMITATION OF ABSTRACT
Unclassified	Unclassified		

NSN 7540-01-280-5500

Standard Form 298(Rev. 2-89)
Prescribed by ANSI Std. Z39-18
298-102

☆U.S. GOVERNMENT PRINTING OFFICE: 1993 - 728-064/86017